Journal of the Brazilian Society of Mechanical Sciences and Engineering (2023) 45:481
https://doi.org/10.1007/s40430-023-04383-8

REVIEW

A review on recent advancements in an automotive turbocharger rotor system supported on the ball bearings, oil film and oil-free bearings

Narisimha Murty Tammineni[1] · **Rajasekhara Reddy Mutra**[1]

Received: 22 December 2022 / Accepted: 28 July 2023 / Published online: 22 August 2023

Abstract
In recent years, turbochargers have gained importance in the automotive industry, locomotive, and marine applications powered by diesel engines. Also, they are widely implemented in aerospace applications to enhance the engine's performance. The lightweighted turbochargers are implemented in aerospace and automotive industries having a rotational speed above 150,000 rpm; meanwhile, the turbochargers implemented in marine and locomotive applications are heavily sized, with rotational speeds around 30,000 rpm. By recovering waste energy from exhaust gases, the turbocharger provides higher inlet air pressure and mass to the engine and, in turn, boosts engine efficiency and reduces emissions. Bearings such as floating ring bearings, rolling element bearings, hydrodynamic bearings and gas foil bearings are the commonly supported bearings for turbochargers which can operate at higher speeds and are strongly nonlinear. However, while running, the rotor vibrates at sub-synchronous frequencies due to fluid instabilities. Instabilities occur in rotors mainly because of unbalanced, whirl, and whip phenomena of oil. Hence, along with the nonlinear and stability analysis, the thermo-mechanical effects must analyze thoroughly for better performance and improvement in the turbocharger's efficiency. The proposed study thoroughly reviews various analyses for a turbocharger rotor system assisted on the bearings mentioned above with different operating conditions. It explains the influence of the thrust bearing on the turbocharger dynamics. Further, the report includes additional guidelines on research topics that must explore extensively in the upcoming years.

Keywords Turbocharger · Rotor dynamics · Floating ring bearing · Gas foil bearing · Thrust bearing · Rolling element bearings · Hydrodynamic bearings · Oil whirl/whip

List of symbols

c	Clearance of radial bearing
C	Clearance of gas bearing
e	Effective mass eccentricity
e'	Unbalance displacement
H	Film thickness
L	Length of bearing
R	Radius of gas bearing
t	Non-dimensional time
V	Applied voltage
$\overline{H}$	Normalized film thickness
$\overline{P}$	Normalized pressure
$\overline{Z}$	Non-dimensional axial bearing length
C_1, C_2	The inner and outer film radial clearances
C_v	Lubricant-specific heat
D_{j}	Diameter of Journal
D_{ro}	Floating ring outer diameter
m_{c}	Mass of the compressor
m_{t}	Mass of the turbine
P_{a}	Atmospheric pressure
O_{b}	Origin of bearing
O_{j}	Origin of journal
O_{r}	Origin of ring
R_{j}	Radius of journal
R_{ro}	Floating ring outer radius
s_{h}	Shoulder height
U_c	Initial unbalance
Ω_{j}	Angular velocity of Journal
Ω_{r}	Angular velocity of the ring
$h_{\mathrm{i}}, h_{\mathrm{o}}$	The inner and outer oil film thickness

Technical Editor: Jarir Mahfoud.

Rajasekhara Reddy Mutra
rajmech03@gmail.com

[1] Dynamics and Vibration Lab, School of Mechanical Engineering, Vellore Institute of Technology, Vellore, Tamil Nadu 632014, India

p_i, p_o	The inner and outer oil film pressure
Q_i, Q_o	Lubricant leaving flow rate at the inner and outer oil film
r_i, r_o	Thrust bearing inner and outer radius
$\overline{F}_x, \overline{F}_y$	Reaction force of gas bearings
$\overline{F}_0, \overline{F}_1, \overline{F}_2$	Fluid film viscosity integrals
$\overline{w}_t$	Non-dimensional elastic deformation of the foil structure
F_{ub}	Unbalance force
H_j, H_{R_i}	Heat convection coefficients to the shaft OD and the ring ID surfaces
H_c, H_{R_o}	Heat convection coefficients to the casing ID and the ring OD surfaces
K_p, K_d, K_i	Proportional, derivative and integral gains
$\dot{m}_{\theta_i}, \dot{m}_{z_i}$	The lubricant mass flow rates in the circumferential and axial directions
T_d, T_i	Integral and derivative constants
T_s, T_{R_i}	Temperature of the shaft and ring inner diameter surface
T_c, T_{R_o}	Temperature of the TC casing ID surface and ring OD surface
$\frac{\partial h_i}{\partial t}, \frac{\partial h_o}{\partial t}$	The squeeze terms
$\begin{Bmatrix} f_{ix} \\ f_{iy} \end{Bmatrix}, \begin{Bmatrix} f_{ox} \\ f_{oy} \end{Bmatrix}$	The inner and outer oil film forces
$\begin{Bmatrix} F_{ix} \\ F_{iy} \end{Bmatrix}, \begin{Bmatrix} F_{ox} \\ F_{oy} \end{Bmatrix}$	The inner and outer real oil film forces

Subscripts

i	Parameters of inner oil film
j	Journal
o	Parameters of outer oil film
r	Floating ring

Greek symbols

α	Material thermal expansion coefficient
β	Angular extent of sector
γ	Clearance ratio
$\varGamma$	Shear rate
Γ_c	Critical shear rate
θ	Rotor rotating angle around the Z-axis
$\dot{\theta}$	Angular speed
$\ddot{\theta}$	Angular acceleration
θ_o	Angular length of the bearing pad
θ_{amp}	Angular length of the converging gap
$\varLambda$	Bearing number
λ	Fluid circumferential average velocity ratio
μ	Lubricating oil viscosity
μ_*, μ_∞	Viscosity at null and infinite shear rates
ρ	Lubricant density
σ	Load parameter
τ_0	Yield stress parameter
Ω	Angular velocity of the journal

Abbreviations

AFB	Airfoil bearing/foil air bearing
AFJB	Airfoil journal bearing
AFTB	Airfoil thrust bearing
BHP	Break horsepower
CHRA	Center housing and rotating assembly
CHT	Conjugate heat transfer
CLC	Critical limit cycles
FB	Foil bearing
FDM	Finite difference method
FEA	Finite element analysis
FEM	Finite element method
FFRB	Full floating ring bearing
FFT	Fast Fourier transform
FRB	Floating ring bearing
FRGB	Floating ring gas bearing
FTB	Foil thrust bearing
FVM	Finite volume method
GFB	Gas foil bearing
GFJB	Gas foil journal bearing
HDB	Hydrodynamic bearing
ICE	Internal combustion engine
LCC	Load-carrying capacity
OISCM	Oil injection swirl-control mechanism
REB	Rolling element bearing
RFRB	Rotating floating ring bearing
SFD	Squeeze film damper
SFRB	Semi-floating ring bearing
TB	Thrust bearing
TC	Turbocharger
TEHD	Thermo-elastohydrodynamic
TEI	Thermoelastic instability
THD	Thermo-hydrodynamic
TI	Total instability

1 Introduction

Currently, on downsized automotive engines, the practices are aimed at achieving outstanding performance by reducing fuel consumption and adopting a new form of engines that are optimized in size to produce an equivalent amount of power to the larger machines and to abide by laws of the government requiring compliance with emissions standards.

With the ever-reducing demand for emissions and fuel consumption reductions, smaller displacement engines or cylinders with a lesser quantity will reduce the vehicle's weight, leading to lower piston-to-cylinder friction and minimizing all driving-related losses. In addition, greenhouse gases such as carbonic acid (CO_2) and nitrogen oxides (NOx) are related to reducing fuel consumption and emissions. However, this results in lower power of the engine. Furthermore, with the employment of booster devices, the increment in the specific capacity of the machine is possible through the introduction of turbochargers, which can utilize the energy confined by the hot exhaust fumes of the engine. Thus, the efficiency of the motor will increase. Figure 1 depicts the six kinds of turbochargers extensively applied in the automobile sector.

Figure 2 depicts the mean flow of energy in a traditional passenger automobile. The exhaust gases from gasoline and diesel engines may reach temperatures of 950C–1050°C and 820–850°C, respectively, and hence, the energy of enthalpy is exceptionally tremendous but utterly disregarded by the ecosystem. Turbochargers use a proportion of this energy to ramp up and increase the specific power of smaller engines [1]. Even at the lower speeds of the engine, the turbocharger can provide greater torque and make the engine more tranquil. Due to a large ratio of power to weight, better performance can be obtained at extreme elevations. Turbochargers give the ability to much larger ones by converting their energy into horsepower through an increase in power output of up to 40%.

Figure 3 represents the schematic depiction of a turbocharger for exhaust gases which features an actuator, compressor, turbine, and an assembly of rotation centrally housed (CHRA). The rotational shaft consists of dual impellers, i.e., a turbine and compressor wheel on either end assisted by fluid film bearings. The provision of these bearings is to withstand the vibrations in the lateral direction; in addition, the double-acting thrust bearing absorbs imbalances caused by the gas flows of the two impellers in the axial direction. Special attention must be maintained while examining the components since approximately 75% of turbocharger failures are due to the lubrication system and mechanical losses. More details about the working principle

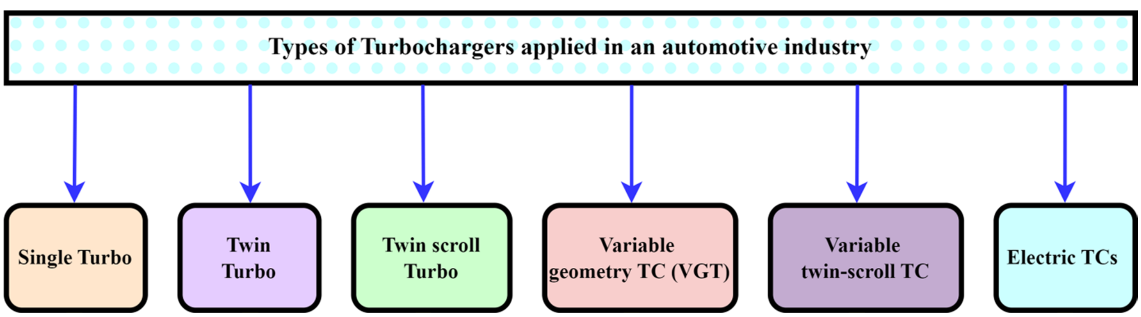

Fig. 1 Different types of turbochargers applied in the automobile sector

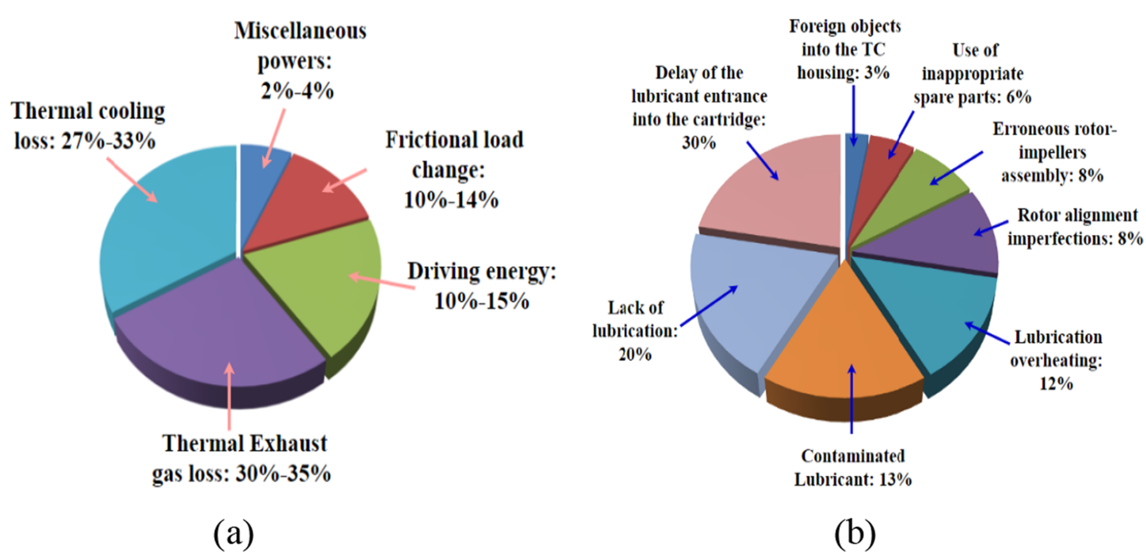

Fig. 2 Schematic view of **a** The energy flow in a passenger car **b** causes turbocharger Failure

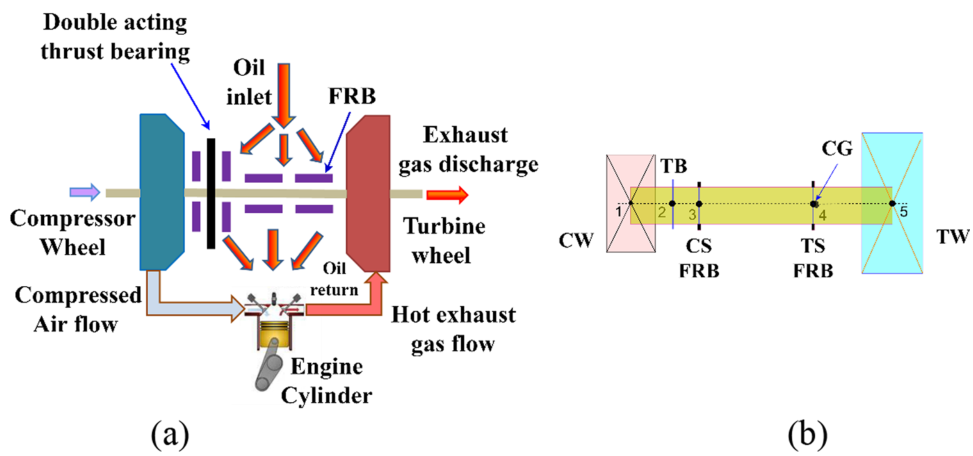

Fig. 3 Schematic view of **a** TC in ICE **b** Finite element model

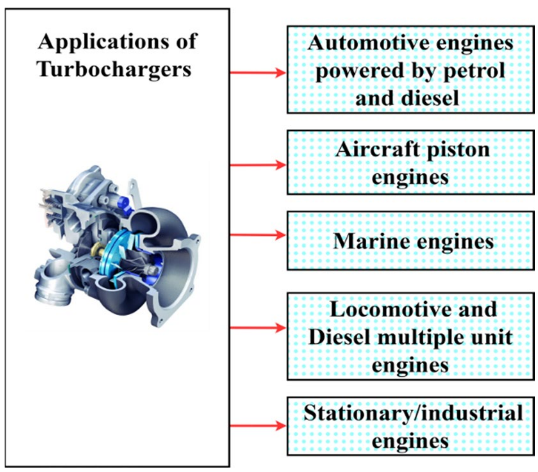

Fig. 4 Applications of turbocharger

and the materials used for the components of a turbocharger can be found in Ref [1, 2].

1.1 Applications of turbochargers

The wide application of turbochargers over the past decade has recently interested many researchers to focus on this field. Commonly available turbochargers can be segmented into two major categories: those intended for application in trucks and automobiles and those used in low- and medium-speed railway traction diesel engines, applications for marines, etc. Cars fueled with gasoline and various custom-required automobiles using turbochargers, as illustrated by the flowchart, are shown in Fig. 4.

1.2 Types of bearings used in turbocharger

During the function of the turbochargers rotor, it can assist by a bearing system consisting of radial and thrust types, as depicted in Fig. 3. Various models of bearings can adapt for rotor assistance, such as rolling element [3], oil-free [4], semi-floating ring [5], and full floating ring [6]. Figure 5 depicts the flowchart for the different bearings used in the turbocharger applications. Figure 6 and 7 illustrate FRB, GFB, rolling and hydrodynamic bearings considered in this review article. Readers can find a detailed theoretical study and applications of FRB and rolling bearings in Ref [7], GFB in Ref [4], and hydrodynamic bearings in Ref [8], respectively.

1.3 Turbocharger failures

Generally, turbochargers will spin at high speeds, such as 200,000 rpm. An increment in the speed (Ω) of the rotor gives rise to rotational forces and leads to rotor excitation due to unbalance (U) as $F_{\mathrm{Ub}} = U\Omega^2$ [7]. Additionally, low production quality and improper tolerances in assemblies lead to high amplitude vibrations, which cause the failure of bearings with raucous. Figure 8 depicts the various causes of the turbocharger's failure.

1.4 Problem statement

As explained in Sect. 1.2, different bearings supporting the turbochargers can exhibit both linear and nonlinear characteristics at high rotational speeds. The operating speed of the turbocharger is very high; even a minor disturbance or vibration can lead to catastrophic system failures. The study of the turbocharger rotor's stability and dynamic analysis varies when it supports on different bearings. Each bearing has other dynamic characteristics based on operating conditions. The linear, nonlinear and thermo-mechanical phenomena must analyze for better stability conditions and excellent engine performance. Hence, this article will direct the readers to glimpse potential problems and upcoming views by reviewing the research performed on the mentioned analysis over the past three decades and the most recent findings to emphasize the path that research and development

Fig. 5 Flowchart for the types of bearings used in the turbocharger

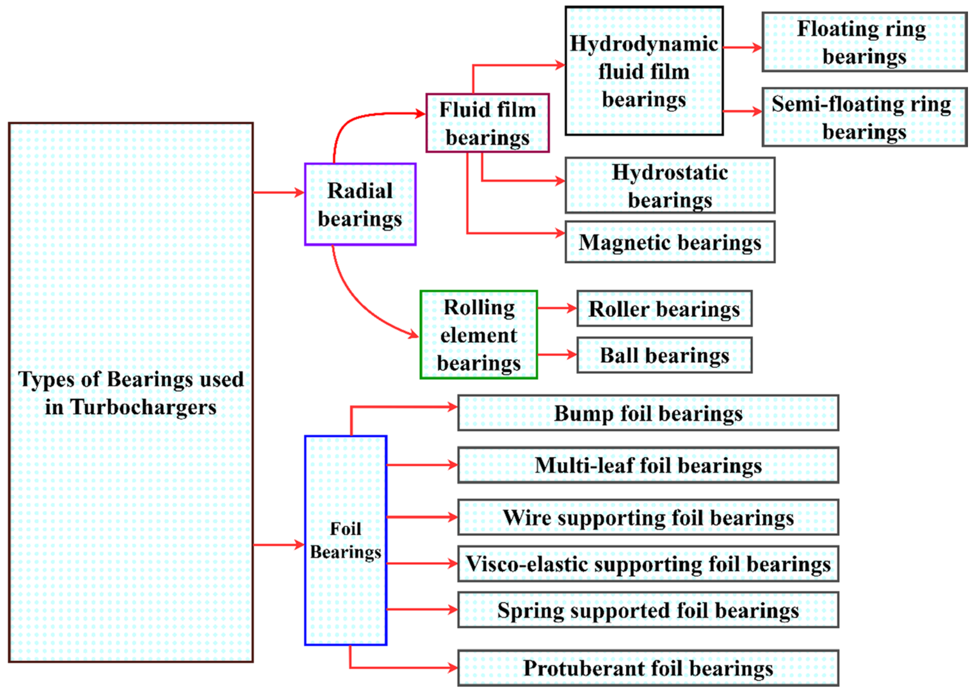

Fig. 6 Schematic diagram of **a** FRB **b** SFRB **c** Gas foil bearing

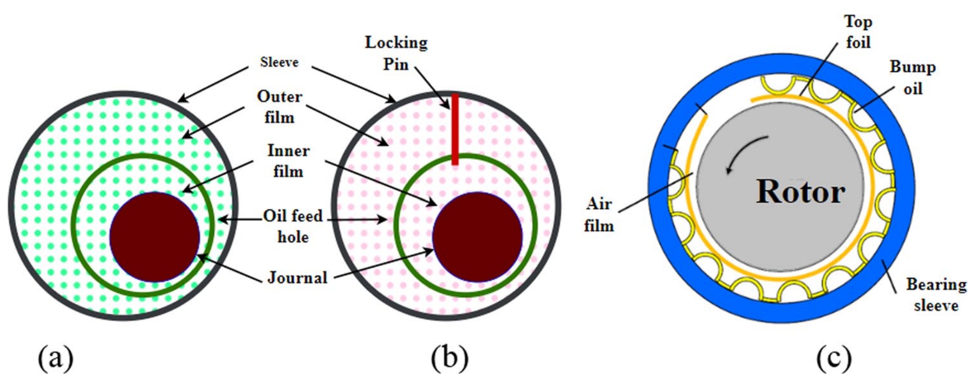

Fig. 7 Schematic view of **a** Ball bearing **b** Hydrodynamic bearing

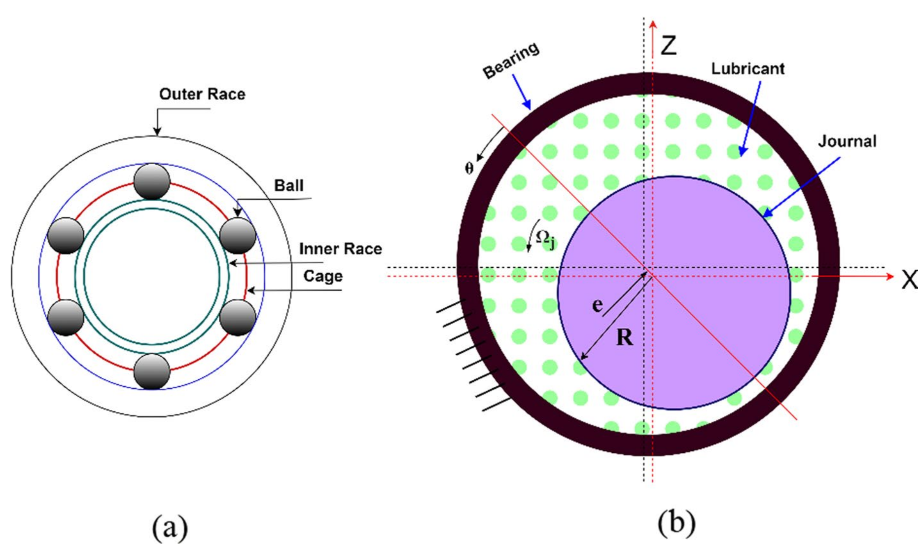

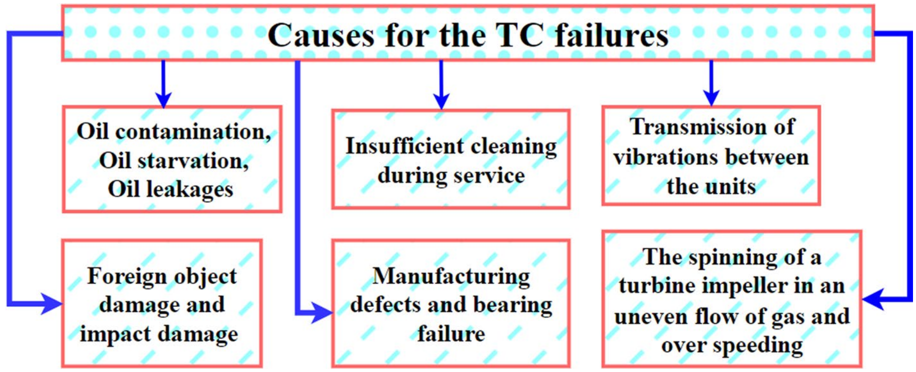

Fig. 8 Various causes for the turbocharger failure

should consider in studying turbocharger dynamics. Figure 9 depicts the flowchart structure for the current article.

2 Stability and dynamic analysis of turbocharger rotor systems

The following section explains the literature survey on the stability and dynamic analysis of turbocharger rotors supported on different bearings, such as floating ring bearings, gas foil bearings, journal bearings and ball bearings.

2.1 Turbocharger rotor system supported on FRB

Generally, the turbochargers of automobile engines typically operate at more incredible rotational speeds and can assist by FRBs. FRBs have a higher load capacity than standard axial groove bearings [9]. Even a small amount of unbalance or defects in manufacturing may produce dangerous and high amplitude vibrations, which can run the system into a highly nonlinear characteristic region. During the run-up, the bifurcation occurs, and they rely heavily upon the bearing parameters and the rotor. These issues can fix by evaluating various nonlinearities to understand the dynamic characteristics of the turbocharger system [10]. The following sections will provide the research conducted in the past on the influences of various parameters on the stability and dynamic characteristics of the system.

2.1.1 Influences of unbalance

Knoll et al. [11] evaluated the FRB-assisted turbocharger rotor stability characteristics by developing a computer time-efficient approach by integrating a multi-body system with the floating bush. They demonstrated the amplitude fluctuation between unstable and stable states and how the unbalance caused the rotor to undergo synchronous vibrations and lower amplitude around the equilibrium point. The large eccentricities could lead to the rigid nature of the two bearings. Hence, in a brief instant, the deflection would increase rapidly in the turbine and compressor. Later, Kirk and Ali [12] suggested a novel technique for improving

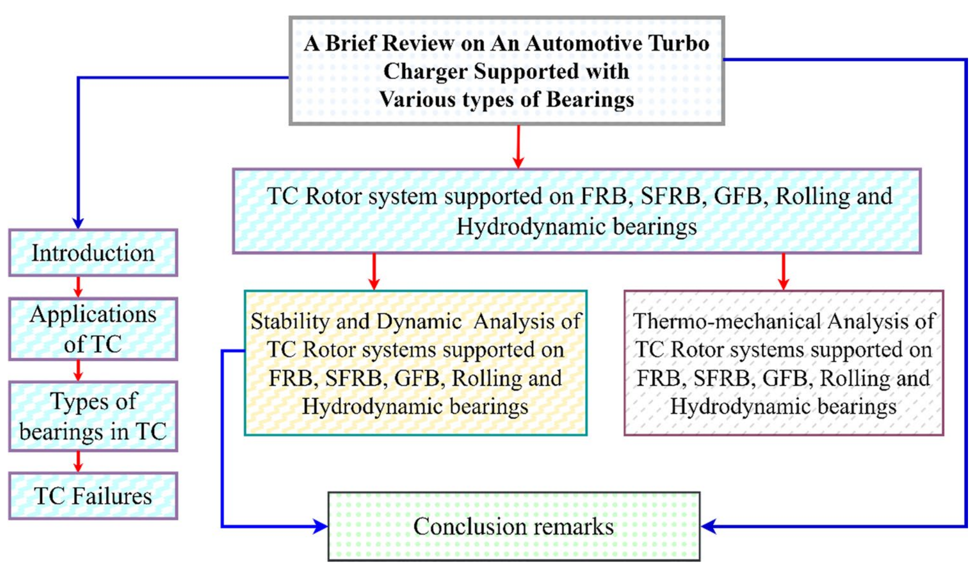

Fig. 9 Flowchart of the structure of the article

dynamic consistency by introducing an unbalance to the rotor of the turbocharger in both wheels to suppress the vibrations, which were subsynchronous by considering the initial unbalance $\left(U_c\right)$ value as 0.108 g mm, along with $e/c = 0.16$. Their linear analysis results reported that when the turbocharger operated at higher speeds, the floating ring's forward mode of whirling would become unstable at the end of the compressor along with the remaining unstable forward modes, i.e., conical and cylindrical types. By inducing unbalance either to the compressor ends or to the turbine ends by a certain amount, they reduced the dominating first mode's amplitude of frequency, which was subsynchronous. In another nonlinear study, Zhang et al. [13] adapted the short-bearing approximation approach [14]. They observed three essential vibration components within the turbocharger's critical operating speed range caused by the rotor's imbalance and the interior and exterior oil film's unstable conditions, i.e., (i) A synchronous vibrational component when the shaft speed equals circular frequency. (ii) A vibrational component that was sub-synchronous when the circular frequency was nearly 40% of the speed of the shaft. (iii) A sub-synchronous vibrational component when the circular frequency was almost 18% of the speed of the shaft. An imbalance of the rotor and greater viscosity of the lubricant might prevent the formation of instability to the extent that the rotor system remains stable throughout a broad range of speeds. They noticed an enhanced damping effect in the exterior oil film and instability in the interior oil film at greater speeds. A prolonged oil whirl effect was noticed in the external oil film. Additional lubrication provided for the interior space increased the damping effect and significantly prevented the exterior oil film from becoming unstable. In another study, by applying various levels of unbalance in the impeller wheels, Bin et al. [15] reported that continuous increments in the unbalance could enhance the rotor's vibration amplitude. The asynchronous nature of the oil film was the leading cause of the extreme vibration. Their analysis revealed that the magnitude of unbalance was an efficient approach to acquiring the lower magnitude vibrations and stabilized operation of a high-speed rotor system. In a recent experimental study, Singh and Gupta [16] emphasized how the unbalance due to rotation and excitations of an engine influences the TC rotor systems. They observed that at elevated speeds, the sub-synchronized vibrations could reduce by the force of inertia developed because of rotational imbalances, which prevail over the forces of nonlinear bearing and excitations of an engine. Equations (1–2) depict the unbalance applied on turbine and compressor wheels [15].

$$F^c_{\mathrm{ub}} = \begin{pmatrix} F^{xc}_{\mathrm{ub}} \\ F^{yc}_{\mathrm{ub}} \end{pmatrix} = \begin{pmatrix} m_c e' \dot{\theta}^2 \cos\theta + m_c e' \ddot{\theta} \sin\theta \\ m_c e' \dot{\theta}^2 \sin\theta - m_c e' \ddot{\theta} \cos\theta \end{pmatrix} \tag{1}$$

$$F^t_{\mathrm{ub}} = \begin{pmatrix} F^{xt}_{\mathrm{ub}} \\ F^{yt}_{\mathrm{ub}} \end{pmatrix} = \begin{pmatrix} m_t e' \dot{\theta}^2 \cos\theta + m_c e' \ddot{\theta} \sin\theta \\ m_t e' \dot{\theta}^2 \sin\theta - m_t e' \ddot{\theta} \cos\theta \end{pmatrix} \tag{2}$$

2.1.2 Influences of oil whirl and whip

When the fluid film bearings in the turbochargers are lightly loaded, and if a viscous fluid is allowed to circulate in the clearance of the bearing with a half speed of the journal as a mean velocity, oil's more incredible rotational speed functions as a source of excitation termed oil whirl [17, 18]. As soon as the rotor attains the first critical speed, i.e., once its angular velocity closes toward twice the natural frequency, the phenomenon of oil whip [19] generates. It will persist with the increment in angular speed since the vibration frequency under self-excitation remains constant and close to the initial resonance frequency. When instability occurs, there is a high probability of vibrations when the whip/whirl frequency is in either mode, and they are subsynchronous [17]. During the whirling motion of the film, energy will transfer from rotor rotation into hydrodynamic film forces responsible for the movement of the nonlinear bearing. When excessive oil's self-excited vibration is with an unbalanced forced response, the turbocharger produces discordant noise, which can lead to turbine or compressor impeller degradation. It would lead to system instability, high vibrations, possible rubbing of the rotor and stator, and hence, possible destruction to the spinning machinery resulting in rotor-bearing system failure, reducing turbocharger operation efficiency and life [20]. Rotors assisted by bearings of fluid film type subjected to the issue of instabilities due to oil whip had already attracted a lot of attention. There are typically two approaches for analyzing such systems. (1) A problem of eigenvalue which results from linearizing the system/systems being modeled, and (2) the detailed model's simulation or numerical integration by using nonlinear differential equations. Several methods proposed by researchers for studying and characterizing the oil whirl phenomena, including shaft frequency and amplitude, oil supply pressure, film pressure, system limit cycles, clearance ratios, Hopf bifurcation analysis, finite element method, run-up and run-down simulations, gyroscopic effects and so on. Myers [21] analyzed fluid film bearings supporting simple rotors subjected to oil whirl with the help of Hopf's bifurcation theory [22] and observed the super- and subcritical bifurcations. They reported that stable orbits could be achieved even at rates greater or lesser than the speed of threshold limits; transitions from stability to instability do not occur gradually. Muszynska [22, 23] also performed similar stability thresholds, oil whirl, and oil whip studies. She noticed three eigenvalues for the rotor-bearing system. She predicted the system's natural frequency, synchronous rotor vibrations and two additional threshold stabilities in the initial zone of balanced critical speeds. Her studies revealed that rotor unbalances were directly influenced by the stability region's width, and oil-lubricated bearings could exhibit multiple regimes of vibration where fluid dynamic forces cause rotor self-excitation. Whirl smoothly transforms into a whip due to the increment in rotational speed, and the shaft's pure rotational motion became unstable and stable for the whirl regime beyond the threshold stability and different threshold stabilities reported stabilization and destabilization predictions. In another study, Shaw and Shaw [24] evaluated the qualitative effects of oil whirl behaviors by considering a rotor provided by an unbalance. With a π film, they adopted a 2D model with an extended bearing approximation to accommodate cavitation. They examined how periodic perturbations lead to Hopf bifurcation, and the rotor speed and system parameters under nonlinear resonance conditions can influence the system dynamics. Jian Ping et al. [25] analyzed a FEM-based continuum model in another study. They reported that the rotor system could fail due to oil whipping phenomena and noticed a more significant reduction in modes resulted in more errors. Later, their experimental results demonstrated that an increment in the speed causes oil whip. The whirl of oil caused double-period bifurcations, and Hopf bifurcations were due to the whip of oil. They suggested that while designing the rotors, both bifurcations should eliminate [26]. In another study, by using horizontal and vertical rotors and run-up and run-down simulations, De Castro et al. [27] reported that subsynchronous whirl was evident to a greater extent in the vertical rotor than in the horizontal rotor but nearly double the natural frequency noticeable from the whipping instability. An increment in the instability threshold occurs due to the increment in the moment of unbalance. Similarly, with the aid of Run-up simulations, Bernhard Schweizer [28] studied the FFRBs supported Laval (Jeffcott) rotor's oil whirl and whip instabilities. He reported that by neglecting the imbalance and gravity, a rotor with a perfectly circular orbit and limit cycle vibrations was often caused by an inner oil fluid film that was frequently unstable initially. Occurrence of oil film instability was noticed in outer film but it does not produce a circle-shaped limit cycle orbit. They noticed that when two limit cycles synchronizing each other cause Total Instability (TI) which were named as the internal (inner) and external (outer) oil whirl/whip synchronization, which could lead to rotor damage.

2.1.3 Influences of various parameters

Kirk et al. [2, 29] experimentally investigated the system's dynamic consistency, threshold speed for linear stability, and transient response for an automotive turbocharger by applying the DyRoBeS© finite element analysis code. For speeds above 100,000 rpm, they reported that the turbocharger could produce a strong displacement response, and compared with the turbine end, the end of the compressor could show an intense whirl. Various modes were noticed, and they suggested refining and upgrading the turbocharger rotor mass distribution could be an alternative approach to improving dynamic performance. Schweizer [30] developed the TC model as a multi-body system for 3D flexibility in another study. By varying the outer fluid film width and by considering a linearized system along with and without the gyroscopic effects, he reported that the whirl and whip of oil's frequencies at the interior and exterior films of the turbocharger system cause the rotor to excite by two modes, i.e., the gyroscopic forward modes in conical and translational. Compared with the other fluid bearings, with the increment in rotational speed, the FRBs were vulnerable to instability due to vibrations generated by self-excitation. In a study, Boyaci et al. [31, 32] noticed the emergence of a low-amplitude limit cycle and bifurcations at both subcritical and supercritical points. The load parameter (σ) and clearance ratio (γ) govern the bifurcation. The lower, higher load parameter causes the super- and subcritical bifurcations; hence, they recommended choosing the load parameter (σ) as low as possible. By employing a numerical continuation approach on plain hydrodynamic bearings and FRBs, they reported that in plain journal bearings, vibrations of the rotor owing to whirl and whip of oil had reduced influence. Also, they noticed an unusual vibration pattern in the case of FRBs with various modes of interaction and occurrence of damage for the rotor in an area called critical limit cycles (CLC). Similar studies were performed by Amira Amamou [33] by controlling the parameter, i.e., journal speed and reported that proper choice in the bearing modulus plays a crucial role in evaluating the threshold speed of rotor stability and sequences of bifurcation. Due to the presence of manufacturing tolerance in FRB, the system would be inconsistent. Hence, it is essential to maintain appropriate ranges for bearing clearances. Their experimental results reported that stability boundaries of the floating ring might yield predictable super- or subcritical-type limit cycles which were stable or unstable [34]. In another study, Gunter and Chen [35] reported that the turbocharger might show instability at lower operating speeds due to the bearing's self-excitation. But, the existence of bearing forces with nonlinear nature could run the rotor with regulated limit cycle motion. An increment in the whirl motion could be possible by the increment in the clearance of the bearing, which leads the rotor to the conical whirling mode. The minor bearing clearances could cause a formation of weld joints between any of the impellers to the journal. Hence, the bushing's greater outer clearance acts as an adequate clearance of plain bearing, which gives rise to instability in the first two modes of whirling and reduces the life of the turbocharger. In another study, Bonello [36] adapted a modal-based technique and revealed that vibrations due to self-excitation were greatly diminished by applying ring rotational limits in the case of FRBs and observed more excellent stability of SFRBs than FRBs. They also observed that if the interior and exterior fluid films deteriorate concurrently, the system exhibits a new phenomenon called total instability (TI), which leads to an increment in the eccentricities of the journal; thus, failure of turbocharger might be possible. Bernhard Schweizer [37] studied the TI phenomena of a TC rotor system by using transient multi-body simulations and calculations of eigenvalues. He reported that the TI could express as dual limit cycles under synchronization. Either increment in imbalance, clearance of outer bearing, the width of inner bearing, or decrement in outer bearing's width, the pressure of oil feed might reduce the threshold speed for TI phenomena. Similarly, Mutra and Srinivas [38] evaluated the turbocharger rotor system's dynamic characteristics during transient operational circumstances. Based on various parametric studies, they reported that angular acceleration and deceleration have negligible influence on system total stability. Still, the changes in clearances and static kind unbalances considerably affect the system. An extensive study by Tian et al. [6, 39, 40] under various conditions such as excitations of the engine and unbalance provided that at lower operating speeds, unbalance and vibrations induced by the engine would significantly impact the response of the rotor. At more incredible rotational speeds, they noticed suppression of the rotor's response by the vibrations generated from the instability of the oil film, and it was sub-synchronous. A run-up and run-down simulation techniques resulted that an increment in the exterior clearance of the bearing could eliminate the CLC vibrations in the size of the exterior clearance and ratios of ring speed. Further increment could initially move the amplitude of vibration to a more significant value, then decrease, and then abruptly rise by following a combo [41]. Mutra and Srinivas [42] studied the dynamic characteristics of a turbocharger rotor system under the combined periodic and emissive forces of ideal nonlinear exhaust gas. They adopted neural network schemes and modified cuckoo search to identify the response and parameters of the system. Based on the experimental and simulation studies, they reported that an increment in the rotor speed could change the critical speeds drastically. Furthermore, the interior oil film influenced the critical frequencies more than exterior film. Tamunodukobipi et al. [43] studied the unstable rotor dynamics of FRBs by utilizing an oil injection swirl-control mechanism (OISCM). They performed tests for various ratios of radius and ratios of clearances with different OISCMs within a particular load. Their test results explored that a larger oil injection angle enhances stability and damping characteristics. They recommended that a swirl-control combination with optimal results, the ratio of clearances, and a well-balanced pressure on the oil supply leads to FRB's better performance. At high rotational speeds, i.e., above 180,000 rpm, turbochargers showed two powerful subharmonic patterns due to the instabilities caused by oil whirl. They pointed out that gyroscopes' effects would play a significant role in such rotor systems. Kamesh et al. [44] studied the gyroscopic effects generated by a rotational movement of a stiff rotor concerning the turbocharger instability due to a conical whirl. They reported that the rotor's angular movement generated a whirl in a conical shape and stabilized by the gyroscopic coefficient could suppress by a threshold value of 0.5. There was no change to this value in the case of practical turbochargers, even for asymmetric rotors assisted by FRBs. In another study, Peixoto and Cavalca [45] pointed out that TB could influence the vibrations in the lateral direction by reducing the amplitudes of vibrations and on FRBs ratios of ring speeds; hence, they must be considered during nonlinear studies of the turbocharger. Furthermore, an increment in the oil film temperature enhances the eccentricities of the bearing and decreases the LCC of the bearing. The thermal studies by Peixoto et al. [46] revealed the existence of lateral-axial coupling resulting from rotations of the thrust collar. Also, they observed that airflow at the compressor's outlet generates pressure fluctuations, which axially emerge in an intense synchronous vibration. Recently, Mutra et al. [47] evaluated the effects of TBs and different stiffness and axial preload under various rotor speeds. They reported that the effect due to the stiffness of TBs was huge, and the influence of preloading was less on the rotor system. At more incredible speeds, various harmonics and frequencies induced due to oil were the causes of significant subsynchronous peaks. The increment in the preload values leads to the emergence of multiple peaks. Figure 10 depicts the geometry and variables of the thrust bearing, and Eqs. (3–4) provide the Reynolds equation for calculating the pressure distribution of TB and the oil film thickness [48].

$$\frac{1}{r}\frac{\partial}{\partial\theta}\left(\frac{F_2}{r}\frac{\partial P}{\partial\theta}\right)+\frac{1}{r}\frac{\partial}{\partial r}\left(rF_2\frac{\partial P}{\partial r}\right)=\Omega\frac{\partial}{\partial\theta}\left(\frac{F_1}{F_0}\right)\frac{\partial h}{\partial\theta}+\frac{\partial h}{\partial t} \tag{3}$$

with $F_0=\int_0^h\frac{1}{\mu}\mathrm{d}x, F_1=\int_0^h\frac{x}{\mu}\mathrm{d}x, F_2=\int_0^x\frac{x^2}{\mu}\mathrm{d}x-\frac{F_1^2}{F_0}$,

$$h=\begin{cases} h_0+s_{\mathrm{h}}\left(1-\frac{\theta}{\theta_{ramp}}\right)+r\left(\varphi_y\sin\theta-\varphi_z\cos\theta\right),\theta\le\theta_{\mathrm{ramp}} \\ h_0+r\left(\varphi_y sin\theta-\varphi_z cos\theta\right),\theta>\theta_{\mathrm{ramp}} \end{cases} \tag{4}$$

Based on the radial profile of the FRB, as depicted in Fig. 11, the dimensionless Reynold's equation, the thickness of the exterior and interior films, the squeeze terms, oil film pressures, and the oil film forces at the exterior

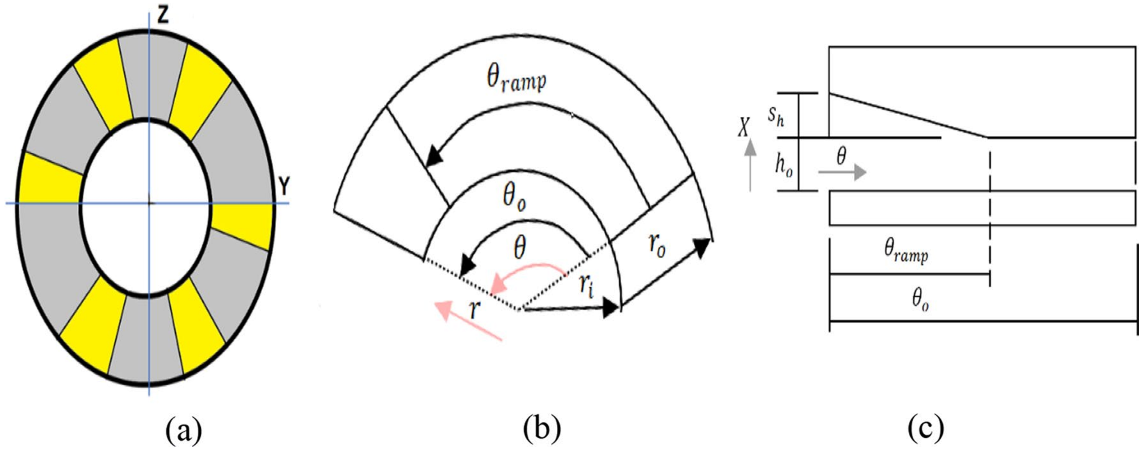

Fig. 10 **a** Thrust bearings fixed geometry, (**b**) and (**c**) variables of thrust bearing

and interior films along with the real oil film forces are provided in Eq. (5–16) [49].

$$\frac{1}{R_{\mathrm{j}}}\frac{\partial}{\partial\theta_i}\left(\frac{h_{\mathrm{i}}^3}{12\mu_i}\frac{\partial p_i}{\partial\theta_i}\right)+\frac{\partial}{\partial Z_i}\left(\frac{h_{\mathrm{i}}^3}{12\mu_i}\frac{\partial p_i}{\partial Z_i}\right)=\frac{\Omega_j+\Omega_r}{2}\frac{\partial h_{\mathrm{i}}}{\partial\theta_i}+\frac{\partial h_i}{\partial t} \tag{5}$$

$$\frac{1}{R_{\mathrm{ro}}}\frac{\partial}{\partial\theta_o}\left(\frac{h_o^3}{12\mu_o}\frac{\partial p_o}{\partial\theta_o}\right)+\frac{\partial}{\partial Z_o}\left(\frac{h_o^3}{12\mu_o}\frac{\partial p_o}{\partial Z_o}\right)=\frac{\Omega_r}{2}\frac{\partial h_o}{\partial\theta_i}+\frac{\partial h_o}{\partial t} \tag{6}$$

$$h_{\mathrm{i}}(\theta_i,t)=C_1-x_j\cos\theta_i-y_j\sin\theta_i \tag{7}$$

$$h_{\mathrm{o}}(\theta_o,t)=C_2-X_r\cos\theta_o-Y_r\sin\theta_o \tag{8}$$

$$\frac{\partial h_{\mathrm{i}}}{\partial t}=-\left(\dot{x}_j\cos\theta_o-\dot{y}_j\sin\theta_i\right) \tag{9}$$

$$\frac{\partial h_{\mathrm{o}}}{\partial t}=-\left(\dot{X}_r\cos\theta_o-\dot{Y}_r\sin\theta_o\right) \tag{10}$$

$$p_{\mathrm{i}}=\frac{3\mu_i}{h_i^3}\left(Z_i^2-\frac{L_i^2}{4}\right)\left\{\left[(\Omega_j+\Omega_r)x_j-2\dot{y}_j\right]-\left[(\Omega_j+\Omega_r)y_j-2\dot{x}_j\right]\right\} \tag{11}$$

$$p_{\mathrm{o}}=\frac{3\mu_o}{h_o^3}\left(Z_o^2-\frac{L_o^2}{4}\right)\left[\left(\Omega_r\mathrm{X}_r-2\dot{Y}_r\right)-\left(\Omega_r\mathrm{Y}_r+2\dot{X}_r\right)\right] \tag{12}$$

$$\begin{Bmatrix} f_{ix} \\ f_{iy} \end{Bmatrix}=-\frac{\sqrt{\left(y_j+2x_j\right)^2+\left(x_j-2y_j\right)^2}}{1-x_j^2-y_j^2}.\begin{Bmatrix} 3x_jV_i\left(x_j,y_j,\alpha_i\right)-\sin\alpha_i.G_i\left(x_j,y_j,\alpha_i\right)-2\cos\alpha_i.S_i\left(x_j,y_j,\alpha_i\right) \\ 3y_jV_i\left(x_j,y_j,\alpha_i\right)+\cos\alpha_i.G_i\left(x_j,y_j,\alpha_i\right)-2\sin\alpha_i.S_i\left(x_j,y_j,\alpha_i\right) \end{Bmatrix} \tag{13}$$

$$\begin{Bmatrix} f_{\mathrm{ox}} \\ f_{\mathrm{oy}} \end{Bmatrix}=-\frac{\sqrt{\left(y_r+2x_r\right)^2+\left(x_r-2y_r\right)^2}}{1-x_r^2-y_r^2}.\begin{Bmatrix} 3x_rV_o\left(x_r,y_r,\alpha_o\right)-\sin\alpha_o.G_o\left(x_r,y_r,\alpha_o\right)-2\cos\alpha_o.S_o\left(x_r,y_r,\alpha_o\right) \\ 3y_rV_o\left(x_r,y_r,\alpha_o\right)-\cos\alpha_o.G_o\left(x_r,y_r,\alpha_o\right)-2\sin\alpha_o.S_o\left(x_r,y_r,\alpha_o\right) \end{Bmatrix} \tag{14}$$

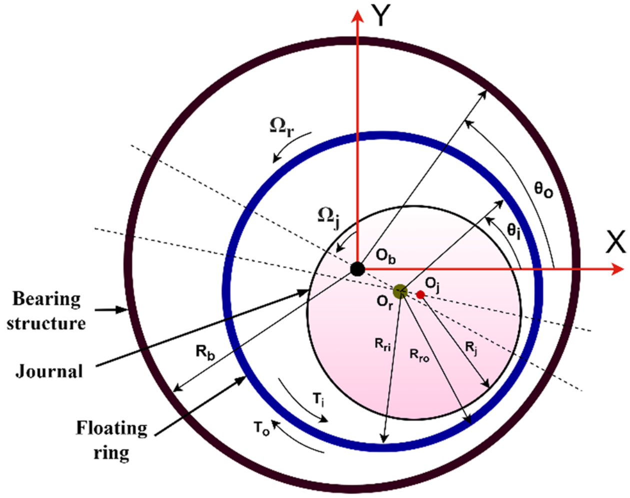

Fig. 11 Radial profile of FRB

$$\left\{ \begin{array}{c} F_{ix} \\ F_{iy} \end{array} \right\} = \mu_i\left(\Omega_j + \Omega_r\right)\mathrm{R_j L}_i\left(\frac{R_j}{C_1}\right)^2\left(\frac{L_i}{2R_j}\right)^2 . \left\{ \begin{array}{c} f_{ix} \\ f_{iy} \end{array} \right\} \quad (15)$$

$$\left\{ \begin{array}{c} F_{ox} \\ F_{oy} \end{array} \right\} = \mu_o\Omega_r\mathrm{R_{ro}L}_o\left(\frac{R_o}{C_2}\right)^2\left(\frac{L_o}{2R_o}\right)^2 . \left\{ \begin{array}{c} f_{ox} \\ f_{oy} \end{array} \right\} \quad (16)$$

Readers can refer to Appendix 2 for the detailed formulation adopted for floating ring bearings.

2.2 Turbocharger rotor supported on gas foil bearings

Over the last decade, oil-free turbomachinery has evolved rapidly in the automotive industry. As depicted in Fig. 12, gas foil bearings (GFBs) are a new-generation type of

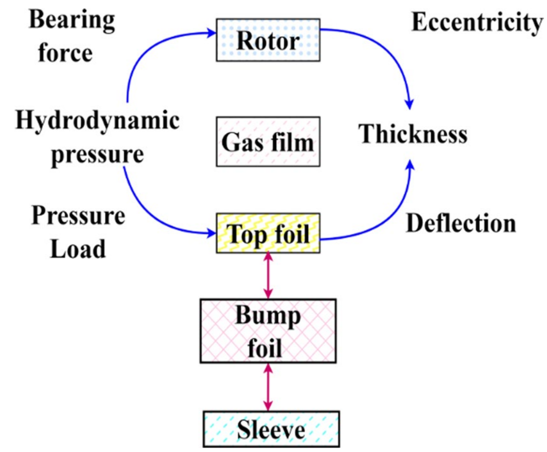

Fig. 13 Model interaction diagram of the GFB

bearings mainly employed to assist the turbocharger rotor system. They have various advantages, including lubricants (air), reduced viscosity value, more incredible rotational speeds, lower frictional losses [50], reduced maintenance requirements, and a remarkable reduction in the system's weight. GFBs applications can be found in compact, high-speed machines such as dental drills and micro-turbines and in massive industrial applications such as turbines and compressors. But, because GFBs have lower dampening, rotors supported by them are prone to instability [51].

Additionally, the bearing will be damaged by startup wear and run-down. Several researchers have worked to enhance the dynamic and stability properties of GFB and addressed its drawbacks. However, the stability up to a specified limit needs to be improved, and the latest technological advances have made it feasible to hybridize the traditional GFB and eliminate its drawbacks. Several methods to minimize the nonlinear phenomena by reducing the computational time

Fig. 12 Bump-type GFB with single pad: **a** The 3D view and **b** The schematic and its corresponding terminology (Reproduced from Ref [56] with kind permission of Elsevier, Netherland)

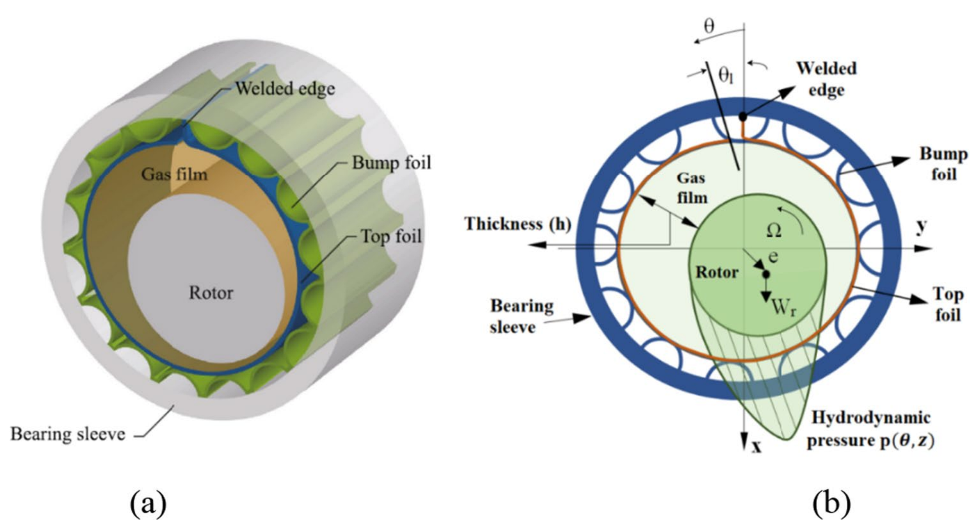

with greater accuracy are proposed in Ref. [52–55]. Figure 13 illustrates the model interaction diagram of the GFB. This section reviews the stability and dynamic characteristics of the rotor supported on foil bearings under friction, unbalance, and other miscellaneous cases.

2.2.1 Influences of friction

In a study of nonlinear analysis, Bou-Saïd et al. [57] noticed that when the rotor's eccentricity attains a maximum value, the system behaves nonlinearly. Providing additional damping to the flexible structure would enhance the level of stability for the flexible bearing. But they did not quantify the damping among the foil and bump due to dry friction. The dry friction generated inside the foil structure could influence the foil structure's dynamic behaviors. Zywica et al. [58] performed experimental and numerical studies and provided guidelines to evaluate the dynamic characteristics of foil bearings by considering dry friction statically and kinetically. Later, Le Lez et al. [59] calculated the forces of dynamic friction at the positions of the top and bottom bumps. With the help of the orbit method, they reported that compared with the rigid-type bearings, the stability characteristics of bearings with the compliant surface could enhance due to the deflection of the structure. The introduction of friction showed a double increment in stability, and the introduction of unbalance revealed that the FBs could carry out unbalanced mass with greater magnitude. In another study, Fangcheng and Daejong [60] reported that nonlinear journal motion could cause by the nonlinear foil structure. For each foil of bump, they proposed a stiffness model with quadratic in type that depended on the total FBs nonlinear stiffness values. Simulation studies showed that dynamic coefficients resulting from the proposed model for lower starting clearances were more significant than the theoretical clearance of the linearized model of stiffness. Earlier research demonstrated that bump foil could make stiffer by the coulomb friction of the foil structure. Later, Lee et al. [61] considered coulomb damping and by simulating the stick–slip motion in the foil bump, they reported that at the resonance condition, FB was much more effective for controlling vibration amplitude. In the structure of foil, GFBs characteristics of damping could mainly generate by the forces of friction depend not only on the topology of the surface and forces acting normally but also on the materials of foil, displacement, and contact surfaces relative velocity. Hence, evaluating the GFB's dynamic characteristics via coulomb friction led to inadequate outputs. Recently, Zywica et al. [62] utilized the coefficients of static and kinetic friction and noticed that the magnitude of force under excitation could significantly influence the FB structure properties. The system's stiffness and damping characteristics could be affected by FB structure with various radial clearances and assembly interference.

2.2.2 Influences of unbalance

Balducchi et al. [63] studied the unbalance responses for two rotors assisted on FBs and demonstrated that FBs could carry unbalances. The addition of unbalance gives rise to the emergence of subsynchronous vibrations. Larsen and Santos [64] explored the unbalance effects theoretically and experimentally for a stiffed rotor assisted on FBs. They observed that the model accuracy mainly depended on the stiffness, deflection, and factor of losses measured depending on the number of bumps carrying the load actively. The level of unbalance and rotation speed mainly influences the sub-synchronous vibrations. Further, Osmanski et al. [65] explained the dynamics of FB by developing a model that depends on a truss representation, which incorporated the mass of foil, and a model of dynamic friction, which considered the dissipation of energy due to friction. The proposed model predicted mode shapes and natural frequencies but

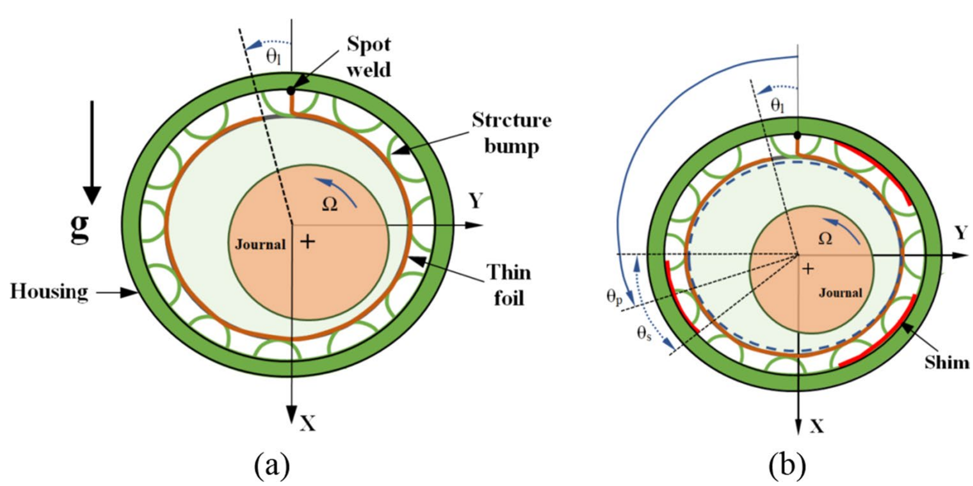

Fig. 14 Schematic views of original GFB and modified GFB with three shims. The top foil leading edge and shims are located relative to the vertical plane as in tests. **a** GFB **b** GFB with three shims

could not capture the unbalance response when the friction comes into play.

2.2.3 Influences of metal shims

Kim and San Andres [66] studied the influences of identical metal shims positioned equally (as shown in Fig. 14). By introducing the preloads mechanically, they observed the increment in natural frequency and LCC due to the influence of fluid dynamic wedge. They reported that GFB with metal shims could result in more excellent stability and performance efficiently. For the increment in threshold stability of bearing, Schiffmann and Spakovszky [67] incorporated selective shimming with variable thickness. They minimized the distribution of pressure for the fluid film by integrating the optimized multi-objective approach. They introduced critical mass as a parameter and observed that FBs with optimized shimming could increase the magnitude twice. The selected critical mass parametric study was well-accepted with the experimental results obtained by San Andrés and Kim [68]. Similarly, Hoffmann and Liebich [69] inserted three metal shims between the sleeve of the bearing and the bump of the GFB elastic structure. By varying the frequency of excitation and amplitude, they reported that due to low Stribeck's effects, the excitation frequency does not significantly influence dynamic stiffness. However, the lower displacements and greater preloads dynamically and statically resulted in greater stiffness and energy dissipation. The slip phase extended by the shims resulted in a high amount of dissipation in the energy; hence, it could gradually enhance the damping. Furthermore, they found that the self-excitation of the fluid film could be a critical resource for nonlinear subharmonic whirling [70]. The introduction of shims enhanced the dynamic characteristics, and the more excellent value of self-excitation was obtained [69].

Turbomachinery like turbochargers, gas turbines, etc., equipped with thrust pads, as depicted in Fig. 15a, must endure the forces which developed axially because of the difference of pressure among the impeller sides, i.e., on the sides of the compressor wheel and turbine wheel. The rotor attitude can also be upheld and decided by the thrust pad. In practical systems, the stiffness and damping of the bearing can be enhanced by this. Hence, the dynamic properties of the FTB must analyze in detail. In a study, Heshmat et al. [71] estimated the deformation and displacement of bump foil by adapting the modeling of FEA and FDM for FTB with an improved bearing geometry as $\beta = 1 \text{and} \theta_e = 45°$. They generated the pressure gradient using the thrust bearing with a plane of inclination, as depicted in Fig. 15b. Later, Ku [72] studied the dynamic properties of FTB adapted with bump foil or strips of corrugated foil in the surface of compliance. For various operational scenarios for the strips of foil bump, he measured the equivalent coefficients of damping and structural dynamic stiffness. From the comparative studies, he reported that an increment in the static load and a decrement in the displacement amplitude could enhance the structure's stiffness with non-variable damping. Adapting a coating with a significant coefficient of friction, lubricant-coated surfaces, increment in the thickness of foil bump, and proper selection of pivot center location could result in dynamic damping and stiffness of the structure.

In another study, Park et al. [74] evaluated the static and dynamic properties of FTB by considering dual planes in which one was a flat plane and later utilized to increase the LCC with the influence of a physical wedge. Based on the force of friction between the contact points and each bump deflection by a uniformly applied load, they observed a decrement in the magnitude from fixed to free end and a proportional relation between the damping and stiffness. An increment in the ratio of eccentricity and bearing number

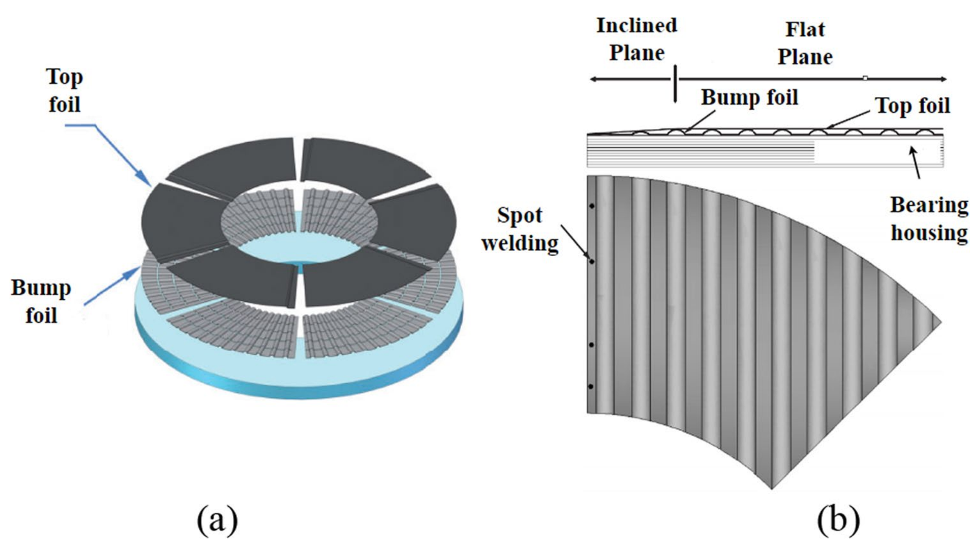

Fig. 15 **a** Fundamental structure of a bump-type GFTB [73] **b** The configuration of the AFTB [74] (Reproduced from Ref [73] with kind permission of SAGE journals, USA) and (Reproduced from Ref [74] with kind permission of Elsevier, Netherland)

or a decrement in inclined parts gradient enhances the torque of the bearing and the load, respectively. They also reported that the dynamic properties mainly depend upon the greater bearing number, and more significant rotor tilt could enhance the generation of torque for bearing and the load because of the decrement in the gradient thickness of the film. In another study, Zhou et al. [75] considered viscoelastic natured supports and observed that either increment in the load axially or decrement in the thickness of the bottom foils could increase the stiffness of the bearing structure. When forces with substantial magnitude and fickle nature acted on the turbomachinery with greater efficiencies like two-stage compressors, FTBs would become essential. In an experimental analysis, Balducchi et al. [76] considered the static load and frequency of excitation in the range of 30 N to 150 N and 150 Hz to 750 Hz. They reported that an increment in the excitation frequency enhances the stiffness dynamically and lowers the damping equivalently. Meanwhile, they noticed the increment in stiffness and damping with the increment in static load. An increment in the static load could enhance the viscous damping; meanwhile, an increment in the excitation frequency could decrease it. In recent, Lehn et al. [77] studied the effectiveness of AFTBs for distorted, aligned and misaligned operation conditions. They adopted the Reissner–Mindlin-model shell concept and modeled the exact geometry of the bump foil. By the comparative studies between the rigid and foiled air-type TBs, they reported that for a perfectly parallel alignment of the base plate and the rotor disk, AFTBs could have a minimized load capacity than rigid-type TBs caused by the sagging influence of top foil and the deformations in the foil bump unequally. Reynolds's equation to obtain the governing equation for GFBs, the non-dimensional film thickness and the bearing forces are presented in Eqs. (17–20) [78].

$$\frac{\partial}{\partial\theta}\left(\overline{PH}^3\frac{\partial\overline{P}}{\partial\theta}\right)+\frac{\partial}{\partial\overline{Z}}\left(\overline{PH}^3\frac{\partial\overline{P}}{\partial\overline{Z}}\right)=\Lambda\frac{\partial\left(\overline{PH}\right)}{\partial\theta}+2\Lambda\frac{\partial\left(\overline{PH}\right)}{\partial t} \tag{17}$$

where$\Lambda=\left(6\mu\Omega/P_{\mathrm{a}}\right)(R/C)^2;\overline{Z}=Z/R;\overline{P}=P/P_{\mathrm{a}};\tau=\Omega t;\overline{H}=H/C;x=R\theta$

$$\overline{H}=1+\overline{\varepsilon}_x\cos(\theta)+\overline{\varepsilon}_y\sin\theta+\overline{w}_t \tag{18}$$

$$\overline{F}_x=-\int_0^{2\pi}\int_0^{L/R}\overline{P}\left(\theta,\overline{Z}\right)\cos(\theta)\mathrm{d}\theta\mathrm{d}\overline{Z} \tag{19}$$

$$\overline{F}_y=-\int_0^{2\pi}\int_0^{L/R}\overline{P}\left(\theta,\overline{Z}\right)\sin(\theta)\mathrm{d}\theta\mathrm{d}\overline{Z} \tag{20}$$

2.3 Turbocharger rotor supported on journal bearings

The excellent load capacity, greater reliability, extended life, and operation at more incredible speeds made the journal bearings (JBs) implemented in various engineering applications like power, automobiles, etc. The following section reviews the influences of viscoelastic supports combined with journal bearings and multiple parameters on the turbocharger rotor system's stability and dynamic characteristics.

2.3.1 Influences of viscoelastic supports

In a study, Dutt and Nakra [79] and Kulakarni et al. [80] adopted a Jeffcott rotor and assumed the supports with three models: elastic, Voigt and four-element viscoelastic types. Their results demonstrated that enhancing the stability threshold, minimized unbalance, and vibration amplitude could be possible for a rotor-bearing system by providing viscoelastic supports. Later, Dutt and Nakra [81] adopted polymeric-type bearing support and minimized the responses due to unbalance over a greater frequency range. Further, by incorporating the gyroscopic effects, they demonstrated that unbalance could be minimized by adequately selecting damped viscoelastic supports [82]. Montagnier and Hochard [83] also validated the same results and confirmed the initial identification of materials with accurate damping for stabilized threshold limits. In another study, Shabaneh and Zu [84] assumed Kelvin-Voigt viscoelastic model and reported that incrementing the viscoelastic loss coefficient could enhance the natural frequency and minimize the vibration decrement. An increment in the fundamental frequency was noticed with the increment of viscoelastic stiffness up to a certain level. In another study, Reddy and Srinivas [85] developed a FEM model demonstrating how viscoelastic support influences the rotor's overall dynamics. Recently, Ribeiro et al. [86] developed a hybrid model incorporating mass in addition to oil bearings and viscoelastic supports. Their results demonstrated that hybrid support could minimize unbalanced amplitude response and the anisotropic stiffness nature of the system. A reduction in the vibration amplitude of 68% was noticed between the models. In addition, the hybrid support does not exhibit any instabilities throughout the spectrum of spin speeds.

2.3.2 Influences of different parameters

Nonlinearity occurs in the journal bearings due to parameters like surface roughness, pad rubbing, etc. The constraints of the manufacturing procedures result in the surfaces of the journal and bearing having an inherent roughness. This factor contributes to the dampening of a system's dynamic response. In a study, Ramesh and Majumdar [87] studied how the surface roughness pattern influences the stability characteristics of a rotor system. They noticed the stability variation with roughness patterns and ratios on the journal and bearing surfaces. Also, they reported that the bearing *L/D* ratio was the determining factor in the degree to which the fluctuation could occur. In another study, Turaga et al. [88] studied the influences of surface roughness on the rotor's transient stability by developing a FEM model. By obtaining the numerical solutions with Fourth-order Runge–Kutta technique, they reported that Surface roughness patterns along the transverse and longitudinal direction could enhance and reduce the system stability, respectively. Lin [89, 90] studied the nonlinear nature of journal bearings by adapting Hopf's bifurcation theory. They reported that roughness patterns along the longitudinal direction could enhance the system's stability and minimize the size of super- and sub-CLC. In another study, by comparing the linear and nonlinear methods, Sinhasan and Goyal [91] investigated the dynamic characteristics of plain JB with non-Newtonian-type fluid. Their results demonstrated the stable and unstable responses for both linear and nonlinear models. Later, Jagadeesha et al. [92] studied the combined influence of non-Newtonian fluid with 3D surface roughness and reported that non-Newtonian fluid could reduce the ratio of minimum film thickness. Further, Kushare and Sharma [93] studied the stability characteristics of worn hybrid JB combined with non-Newtonian fluid. They confirmed the significant influence of non-Newtonian fluid on the system stability and vibration orbits at low load conditions.

2.4 Turbocharger rotor supported on ball bearings

Journal bearings have traditionally been a standard component of turbochargers, providing support for rotor assemblies. On the other hand, REBs are quickly becoming the bearing of choice in turbochargers as a substitute for journal bearings [94]. Even though they are the most delicate elements, they are vital for the efficient functioning of rotating equipment. Applications of REBs can be found in the TCs of automobiles, engines of gas turbines, turbopumps in cryogenic engines, etc. REBs turbocharger feature minimal friction and reacts instantly to engine power variations. They can withstand the stresses of thrust loads in various environments where conventional thrust bearings would fail. The nonlinearity in REBs can occur due to unbalance, damping, internal clearance, stiffness, bearings preload, and the quantity of rolling elements. This section reviews the stability and dynamic characteristics of the rotor supported on REBs under the effects of unbalanced and preloading cases.

In actual practice, the accumulation of imbalanced pressures is a result that cannot be avoided. Eliminating the imbalanced effect in a rotor-bearing system is a complex operation that has to be accomplished. In addition, the impact of being imbalanced can only be mitigated to a certain degree by using effective balancing techniques, but it cannot be eliminated. By considering the imbalanced forces, several different investigations have been carried out. In a study, Tiwari et al. [95] investigated the influences of unbalance combined with the interior radial clearance. They concluded that multiple frequency excitations could produce the existence of unbalanced forces. The more significant components of sub-harmonics were generated due to a more substantial clearance Later, Gupta et al. [96] performed similar experiments with the shooting method and demonstrated that increasing the stiffness ratio could improve the nonlinearity and lead to instability at various rotation speeds. In another study, Harsha and Kankar [97] showed that an increment in ball quantity could make the system stiffer. Further, Harsha [98] combined speed fluctuation influences with unbalanced forces. With the aid of Poincare's maps, he observed the doubling of period and intermittence mechanism, which could lead to chaos, which was further validated and confirmed by Chen [99]. The analytical and experimental study of Ashtekar and Sadeghi [100] demonstrated the influences of preload and unbalanced on the TC rotor system.

In the case of turbochargers assisted with REBs, the bearing's stiffness and rotation accuracy can be enhanced by controlling the precise negative operational clearances between the ball bearings and the outer and inner ring raceways. In the interest of accomplishing these objectives, the bearings have been applied by an internal load, termed preload, which could influence the characteristics of REB. However, bearing preload research is scarce. In a study, Alfares and Elsharkawy [101] examined the influences of axial preloading on the system dynamics. They reported that decrement in the amplitude levels of vibration could be possible by applying initial preload axially. In another study, Bai and Xu [102] pointed out the significance of axial preload and how it enhances the system's stability. Further, Bai et al. [103] investigated the system's stability by employing a bearing model with 5 DOF. They demonstrated that eliminating unstabilized periodic characteristics could be possible by providing sufficient increased axial preload. Gunduz et al. [104] observed that vibration responses were influenced by the bearing's initial preloads, which caused the stiffness matrix's diagonal and off-diagonal elements to change majorly. In another study, Conley et al. [105] reported that the compressor end could bear the maximum thrust load, and friction could increase with the increment in axial load. They noticed an increment in the thrust load with the increment in TC back pressure. Later, Conley and Sadeghi [106] conducted similar experiments and reported that the dynamics of each bearing element could significantly affect by the whirl. They also demonstrated the ball bearing preloading's relevance in ensuring smooth operation. Applying a minimum axial load on the ball bearing indicates the destabilizing effect of the whirl. Recently, Conley and Sadeghi [107] reported that the internal geometry of the bearing could change by centrifugal influences. Hence, a small clearance value would also become a preload at more incredible rotational speeds. Coupling this effect with fewer compliance SFDs would result in reduced sub-harmonics, minimum bearing friction, minimized great load cycles, and overall sliding at the contacts of the ball race, resulting in a greater life span.

2.5 Critical inferences for the stability and dynamic analysis

- At higher speeds, damping effects for the exterior oil film can increase by the lubricant's supply pressure, which creates the instability of the interior oil film. Increasing the internal clearance can enhance the speed range when the interior oil film's unstable condition occurs. Bearing deterioration can be considered as the increment in the area of the internal oil film. Hence, additional lubrication may add to the inner space, which can increase the effect of damping that significantly prevents the exterior oil film from becoming unstable.
- Operating the turbocharger rotor at the third critical speed may generate greater compressive bearing forces and magnitudes, thus, damaging the turbocharger bearing by producing excessive wear. Furthermore, due to wear of running conditions and the absorption of unequal carbon deposits in the impeller wheels, severe vibrations with sub-synchronous nature can generate due to unbalance, leading to failure of the turbocharger rotor system. Furthermore, even if the interior and exterior fluid films deteriorate concurrently, the system exhibits a new phenomenon called total instability (TI), which leads to an increment in the journal's eccentricities; thus, turbocharger failure might be possible.
- Estimating limit cycles are a crucial part of the stability analysis. Steady-state destabilization can achieve by Hopf bifurcation. Saddle node bifurcation is the origin of more incredible magnitude CLC vibrations. Increment in the rotational speeds can eliminate the CLC vibrations in the size of the exterior clearance and ratios of ring speed.
- In the case of FTB, an increment in the tilting angle can decrease the thrust load capacity due to a significant change that can notice in the subsynchronous vibrations caused by the decrement in the rotor rubbing. Also, incrementing various mechanical preloads can increase the onset speed of subsynchronous motions (OSS). An increment in the excitation frequency can dynamically enhance the stiffness and lower the damping equivalently—meanwhile, an increment in stiffness and damping with the increment of static load. An increment in the static load can enhance the viscous damping; meanwhile, an increment in the excitation frequency can decrease it.
- In the case of FTB, an increment in the initial minimum film thickness can quickly lower the toque due to frictional force and the static load. At higher speeds, the film thickness ratio can increase with the increment in static load. An increment in the number of bumps, the larger thickness of foil, and the increased bump height can enhance the static load. With the increment in the initial minimized thickness of the film, the stiffness and damping coefficients can decrease exponentially.
- Enhancement of the stability threshold, minimized unbalance, and vibration amplitude could be possible for a rotor-bearing system by providing viscoelastic supports.

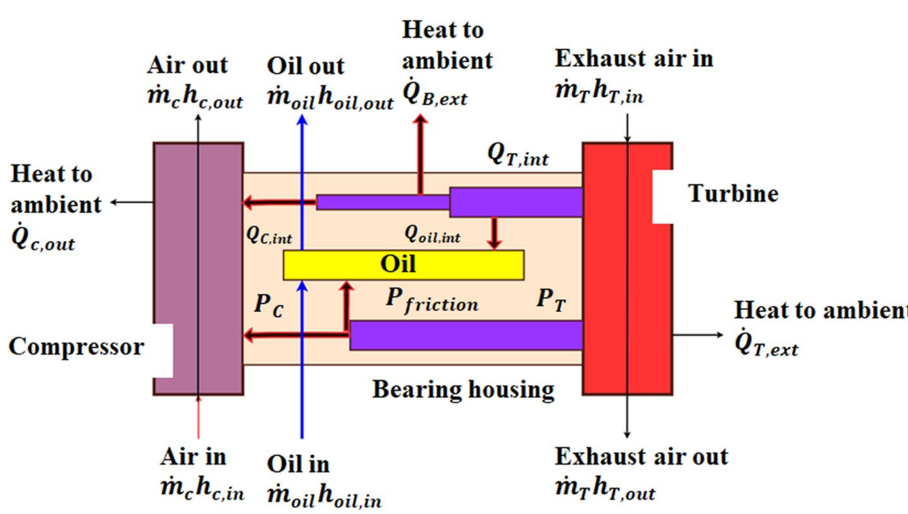

Fig. 16 Schematic view of heat flows in the floating ring-bearing system

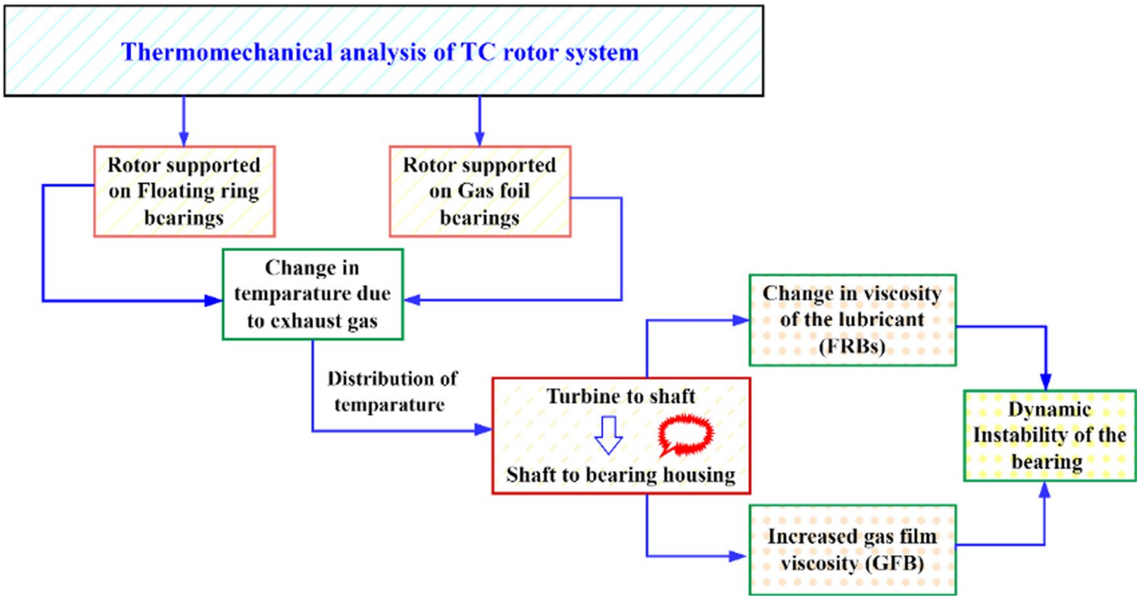

Fig. 17 Schematic view for the thermo-mechanical analysis of turbocharger rotor system supported by floating ring bearings and gas foil bearings

3 Thermo-mechanical analysis of turbocharger rotor system

Automotive turbochargers operating on engine oil lubricants with temperatures of the component above the ambient zone would generate more significant temperature gradients along the radial and axial directions, producing severe stresses thermo-mechanically. The bearings, i.e., both radial and thrust, will function like carrying the load and providing lower frictional assistance. The lubricant takes a significant portion of thermal energy produced by rotating drag and the flow of heat emitted from a heated journal. Figure 16 depicts a schematic view of heat flow in the FRB system. Figure 17 represents the schematic view for the thermo-mechanical analysis of the turbocharger rotor system supported by FRB and GFB. Most of the past works focused on the thermo-mechanical analysis of turbocharger rotors supported on floating ring bearings and gas foil bearings only. The following section reviews the thermo-mechanical analysis of the rotor supported on two types of bearings.

3.1 Rotor supported on FRBs

San Andrés et al. [108] demonstrated the zones of temperature and pressure along with the flow of thermal energy and its distribution in an SFRB system. By quantifying the influences of lubricant feed conditions, clearances of bearing film, and grooves of supplied oil, they reported that the shear power generated could be enhanced by either a more excellent supply of pressure or lower oil temperatures, or greater clearances. Providing additional grooves axially on the interior side of SFRB could improve the dynamic stability and increment in the flow of drawn oil and heat and drag power from the journal.

In another study, Porzig et al. [109] demonstrated the influences of thermally bounded conditions bounded on FFRBs parameter characteristics. Their experimental studies revealed the importance of considering journal temperature's impact on the overall bearing system's functional parameters. They also suggested that non-adiabatic shaft models offer significantly higher accuracy for predicting ring speed than adiabatic models. They demonstrated the importance of an effective heat management system. Due to the complex flow of thermal energy in TCs, interaction among different fluid and solid flows and lubricant flow in the bearing would take a couple by the turbochargers conjugate heat transfer (CHT). Liu et al. [110] utilized the CHT numerical simulation. They noticed a strong temperature gradient during the system run and reported that the temperature could reduce the system's stiffness, leading to intrinsic frequency decrement, especially for higher-order frequencies. They demonstrated the importance of predicting the dissipation of damped internal energy in the temperature zone for better rotor dynamic characteristics. TRIPPETT and Li [111] studied the influences of different bearing characteristics on the speeds of the ring by employing an isothermal bearing approach. They reported that the stability of the bearing, loss of energy, and load capacity relied on the speed of the ring. The effects due to thermal conditions could influence the FRB's performance and the reduction of ring speed. Later, Clarke et al. [112] studied the feasibility of using FRB in the power-generators. The traditional FRB steady-state model included the thermal influences, interior and exterior film heat, mass transfer, and recirculation of oil along the circumference of the bearing. By adopting the least squares technique [113], they calculated the external film's ring speed and eccentricity ratio. Their comparative studies between an iso-viscous model and different thermal models reduced oil viscosity in the interior film and reduced the loss of power.

Responses for transient and steady-state conditions of a turbocharger assisted on FRBs were predicted by San Andrés and Kerth [114], in which they integrated the analysis of thermal flow with nonlinear rotor dynamics by including the heating influences of lubricant and changes in the clearances of bearing due to the consumption of power by the bearing. Their analysis resulted in an increment in the journal speed that could decrease the assumed ring speed ratios due to the thermal influences on the viscosities of the film and clearances during operation. Emerge of aerodynamic loads was noticed in the volute of the compressor due to uneven distribution of pressure. Further, San Andrés s et al. [115] predicted the zones of pressure and temperature in the (S) FRB system by a thermo-hydrodynamic analysis. Their studies revealed that with the vital flow of heat into the interior film from the journal across all the shaft speeds, the lubricant's streams could carry greater than 70% of thermal energy from the input of total energy, and the remaining could conduct via casing of turbocharger. This distribution of thermal energy could justify by feeding a sufficient flow of lubricant to the bearing system. Equation (21–28) provides the corresponding Reynolds equation, the bulk-flow thermal energy transport equation for the inner and outer film, the lubricants leaving flow rate, and changes in the clearances during operation for each interior and exterior film.

$$\frac{1}{R_{\mathrm{j}}^2}\frac{\partial}{\partial\theta}\left(\frac{h_{\mathrm{i}}^3}{12\mu_i}\frac{\partial p_{\mathrm{i}}}{\partial\theta}\right)+\frac{\partial}{\partial Z_i}\left(\frac{h_{\mathrm{i}}^3}{12\mu_i}\frac{\partial p_{\mathrm{i}}}{\partial Z_i}\right)=\frac{\Omega_j}{2}\frac{\partial h_{\mathrm{i}}}{\partial\theta} \tag{21}$$

$$\frac{1}{R_{\mathrm{o}}^2}\frac{\partial}{\partial\theta}\left(\frac{h_{\mathrm{o}}^3}{12\mu_o}\frac{\partial p_{\mathrm{o}}}{\partial\theta}\right)+\frac{\partial}{\partial Z_o}\left(\frac{h_{\mathrm{o}}^3}{12\mu_o}\frac{\partial p_{\mathrm{o}}}{\partial Z_o}\right)=0 \tag{22}$$

where $\mu=\mu_\infty+\dfrac{\mu_*-\mu_\infty}{1+|\Gamma/\Gamma_c|}$

$$C_v\left[\frac{\partial}{R_{\mathrm{j}}\partial\theta}\left(\dot m_{\theta_i}T_i\right)+\frac{\partial}{\partial Z_i}\left(\dot m_{z_i}T_i\right)\right]+H_{\mathrm{R_i}}\left(T_i-T_{\mathrm{R_i}}\right)+H_j\left(T_i-T_s\right)=\Phi_i \tag{23}$$

$$C_v\left[\frac{\partial}{R_{\mathrm{o}}\partial\theta}\left(\dot m_{\theta_o}T_o\right)+\frac{\partial}{\partial Z_o}\left(\dot m_{z_o}T_o\right)\right]+H_{R_o}\left(T_o-T_{R_o}\right)+H_C\left(T_o-T_s\right)=\Phi_o \tag{24}$$

$$Q_i=2\int_0^{2\pi R_i}\left[-\frac{h_i^3}{12\mu_i}\frac{\partial p_i}{\partial z}\right]_{z=L_i}dx \tag{25}$$

$$Q_o=2\int_0^{2\pi R_i}\left[-\frac{h_0^3}{12\mu_0}\frac{\partial p}{\partial z}\right]_{z=L_o}dx \tag{26}$$

$$C_i=C_{i*}-\alpha_jR_{\mathrm{j}}\Delta T_j+\alpha_RR_{\mathrm{R_i}}\Delta T_R \tag{27}$$

$$C_0=C_{0*}-\alpha_jR_{\mathrm{R_0}}\Delta T_R+\alpha_BR_B\Delta T_B \tag{28}$$

Readers can refer to Appendix 2 for the detailed terminology in the following equations [108].

In a high-speed rotor-bearing system, strong coupling existed between the mechanical performance and thermal behaviors. In earlier studies, San Andrés and Kerth [114] applied 2D thermo-hydrodynamic (THD) methodology along with the equation of Reynold and investigated the turbocharger rotor performance. For various rotation speeds, the heat flow between the film of oil and the bearings components was calculated [115]. However, the oil film's conventional 2D THD model could not foresee the behaviors of the oil film because of the presence of thermally bounded and undeveloped layers. Hence, the 3D THD approach was applied to obtain greater accuracy, which may find rare in the current research. Li et al. [116] studied the thermo-hydrodynamic (THD) characteristics of a turbocharger system by developing a 3D model which undertook the transient 3D thermal equation and Dowson equation for calculating the field of pressure as given in Eq. (29–30). Based on the simulation and experimental studies, they noticed four sub-synchronous frequencies under excitation in conical and cylindrical bending shapes in the inner and outer films. Solid components significantly aided the lubricating system's heat transmission. For greater amplitudes, the variation in the rotors and ring temperatures could influence the change in the thermal expansion and the clearances of the oil film. Similar studies was performed by Liang et al. [117] by including the non-Newtonian oil lubricant in the model. They reported that the conduction of heat between the ring and rotor is equivalent to the heat flow of oil film. They also pointed out that heat transfer among the two bearings should not neglect. In the case of interior oil films, they observed that the clearances of the internal film could significantly change by the thermal expansion of the solid components. Recently, San Andrés et al. [118] experimentally demonstrated that the ring temperature varies in all directions, mainly axially, due to the conduction of heat from the thrust bearing into the ring. The total energy flow equals the viscous drag power losses from the inner film in the radial bearing and the thrust bearing plus the heat soaked from the shaft. Therefore, adequate clearance and suitable material selection could provide convenient thermal management, avoiding elevated temperatures that cause the engine's oil failure due to burn and flash.

$$C_\varsigma \frac{\partial(\rho T)}{\partial t} + C_v\left[\frac{\partial(\rho u T)}{\partial x} + \frac{\partial(\rho v T)}{\partial y} + \frac{\partial(\rho w T)}{\partial z}\right] - k_r \frac{\partial^2 T}{\partial z^2} = \mu\left[\Gamma_x^2 + \Gamma_y^2\right] \tag{29}$$

$$\frac{\partial}{\partial x}\left(J\frac{\partial P}{\partial x}\right) + \frac{\partial}{\partial y}\left(J\frac{\partial P}{\partial y}\right) = U\frac{\partial}{\partial x}\left(H - \frac{J_1}{J_O}\right) + \frac{\partial H}{\partial t} \tag{30}$$

3.2 Rotor supported on gas foil bearings

Lee and Kim [119] developed a model of THD in detail by evaluating the air film's temperature, foil of bump and top, the sleeve of the rotor and bearing with the aid of equations, i.e., Reynolds, 3D energy, and balance of heat for the system of rotor bearing and its subsystems. Their proposed THD model demonstrated that the bearings sleeve and the rotor temperature could exhibit a parabolic shape when plotted against the rotor speed. Furthermore, they observed the changes in clearance due to the foil structure's thermal development accounted for just 1% of nominal clearance and an increment of roughly 20% of the nominal clearance due to the rotor expanding owing to heat and centrifugal force. Equations (31–32) depict the proposed thermodynamic model's Reynolds and energy equations.

$$\frac{\partial}{\partial x}\left(\frac{ph^3}{\mu(T_f)T_f}\frac{\partial p}{\partial x}\right) + \frac{\partial}{\partial z}\left(\frac{ph^3}{\mu(T_f)T_f}\frac{\partial p}{\partial z}\right) = 6U\frac{\partial}{\partial x}\left(\frac{PH}{T_f}\right) \tag{31}$$

$$\begin{aligned}\rho(T)c_p(T)&\left(u\frac{\partial T}{\partial x} + v\frac{\partial T}{\partial y} + w\frac{\partial T}{\partial z}\right)\\ &= k(T)\left(\frac{\partial^2 T}{\partial x} + \frac{\partial^2 T}{\partial y} + \frac{\partial^2 T}{\partial z}\right)\\ &\quad + \left(u\frac{\partial p}{\partial x} + v\frac{\partial p}{\partial y}\right) + \Phi\end{aligned} \tag{32}$$

with $\Phi = \mu(T)\left[\left(\frac{\partial u}{\partial y}\right)^2 + \left(\frac{\partial w}{\partial y}\right)^2\right]$

Later, San Andres and Kim [120] considered a thermal model with lumped parameters and presented a 2D THD bulk-flow model, which included the convection of heat and conduction paths along and out of the journal and bounded bearing surfaces. They included the coupling of thermal structures, which could influence the properties of structure and bearing components' sizes, such as journal diameter and minimum clearances. They reduced the coefficients of heat transfer by using the Reynolds-Colburn analogy, which adopted between the fluid friction and fully developed flow of heat transfer. The readers can refer to refs. [121, 122] for validating the mathematical model with the available test data. Lee and Kim [123] developed a 3D-THD model and noticed that the temperature of the thrust disk was speed functioned and parabolic in shape. An increment in the rate could enhance the temperature of the disk's runner. As the speed of the surface was dependent on the disk's radius, the temperature gradient toward the exterior diameter was relatively huge. Thus, the thrust disk and plates thermal expansion lower the clearance of the bearing. Neglecting the thermal expansion for a design of lower clearances of the bearing might be prone to runway thermally. In another study, Aksoy and Aksit [124] adapted an augmented Lagrangian contact model for the bearing components' physical connection and Cooper–Mikic–Yovanovich (CMY) correlation for the thermal contact. They reported that an increment in the shaft speed could rapidly increase the temperature. A greater temperature was observed at the center of the bearing than at the edges, and the occurrence of bearing seizure was noticed. The hot fluid under circulation must replace by the fresh air by employing an axial flow of cooling externally, which might prevent an occurrence of bearing failure because of the requirement in thermal instability. Lehn et al. [125] presented a 3D TEHD model for AFTBs and studied the thermal features by including the thermal expansion effects and axisymmetric Navier-Lame equations. Their results demonstrated that an increment in the speed enhances the AFTBs load capacity up to a certain critical speed and decreases to speed. They proved that the thermal runaway originated from the bending of the disk induced thermally, which would lead to a function of an unfavorable gap. In another study, Kumar et al. [126] investigated the thermo-hydrodynamic characteristics of GFJB under the influence of the slip-flow state. They noticed a lower value of LCC for slip flow due to the generation of lower hydrodynamic pressures. They reported that an increment in the speed would lead to a decrement in the damping coefficients and an increment in the stiffness coefficients. They demonstrated why slip flow must consider while designing the bearings with lower clearances. Recently, Zhang et al. [127] studied the GFTB's thermo-aerodynamic properties by building a thermoelastic coupling model and explained the in-and-out nature of viscosity dissipation on the gas film's temperature rise. They pointed out the importance of viscosity dissipation in the increase in temperature and field of flow for aerodynamic BFTBs. They reported that at dissipated viscosity, the air film's maximum temperature could locate close to the exterior diameter and circumferential outlet, and the velocity gradient could be greater. Their parametric studies revealed that an increase in temperature due to the dissipation of viscosity was responsible for greater than 90% of air film's aerodynamic heating. In an experimental study, Dellacorte et al. [128] conducted durability and performance tests on FBs within a broad range of loads (10–50 kPa) and temperatures (25–650 °C). They reduced the wear and friction by applying PS304, a solid lubricant coating, on the foils of super-alloy nickel-based. With proper additives, they showed an ideal temperature with a bearing life surpassing 100,000 cycles under greater loads. For a better understanding of the influences of load and speed on the temperature, the rise of different temperatures could cause a decrement in the stiffness. Further, Howard et al. [129, 130] experimentally studied the influence of the rise in temperature on FB's damping and stiffness. They observed the decrement in the stiffness to temperature by twice, especially during the temperature increment from 25 to 538 °C. Also, they observed that an increment in the temperature enhances the damping mechanism, which transformed to frictional damping type from the viscous type. In another study, San Andres et al. [131] observed an increment in the equivalent coefficients of viscous damping as 19–26% by an increment of journals temperature from 23 to 263 °C by providing a heater with frequencies of excitation ranging from 50 to 200 Hz. They also observed that the condition might arise due to the faster growth of the journal than the FBs interior surface, resulting in a reduction in the bearing clearance and influencing the preloads increment. A greater increment in the preload enhances the number of bumps active in contact, introduces a greater contact area of sliding, and enhances the damping of the frictional coulomb type. From the experimental analysis results, at elevated temperatures, along with the reduced stiffness [129, 130], they observed the existence of a significant temperature gradient in the axial direction. Hence, the LCC could be affected, and the combined effects of load and thermal conditions could influence the damping mechanism. One significant concern was the foil material's localized overheating because of the viscous heating, which could not be uniform inside the air film during the bearing operation at greater speed and loads, while in performance, three factors affect the interior temperatures: the ambient environment's temperature, heat emerges in the thinned film of air due to viscous shearing, and the work of compression in which the journal pumps air to the zone of higher pressure from ambient [132]. In GFBs, an increment of viscosity with an increment in the air's temperature could emerge thermal instability [133]. The formed thermal gradient could wrap the top foil to a single point, where the disruption occurs during film formation. Minimizing the available air film to support the load, which results in contact with rubbing at more incredible speeds, could lead to catastrophic failure called thermoelastic instability (TEI) [134]. TEI could associate with the buildup of heat in the zone of high stress caused by the frictional heat flow in an uneven stress field. On the verge of instability, a greater amount of localized temperatures caused by the unrestrained increment in temperature emerges localized hot spots, degradation of the material, and failure eventually [135]. Despite the scarcity of experimental findings, several reports highlighted that in FBs, the temperature rise could emerge as TEI. Zywica et al. [136] conducted multiple experiments by increasing the speed of the rotor up to 15,000 rpm for a duration of 55s and obtained the thermal equilibrium by maintaining the same rate. Even after the 300s, they noticed an increment in the bearing temperature without any stabilization. The top foil lower portion attained a temperature of 130°C, and the journal temperature reached 200 °C. Persistent hot spot marks were discernible at several locations of the foil top after the rotor stoppage. The authors cited rotor overload as the cause of failure. In another study, Lee et al. [137] conducted experiments on FB without a jacket of cooling and noticed the TEI at an operating load and speed of 97.7 N at 35,000 rpm, respectively. As a result of this instability, the temperature of the foil top shot up to well over 100 °C by creating localized hot spots. Hence, it was mandatory to evaluate the TEI at the design stage to reduce the failure of the FB. Recently, Samanta and Khonsari [138] provided an analytical solution by predicting the critical speeds responsible for the TEI of FB. They calculated the heat wave's amplitude and elastic deformation by perturbation approach and compared it with the deformation of the entire surface due to pressure and heat. The model also revealed that the critical speeds of TEI would mainly depend on the operating parameters of bearings, such as speed, load, bearing and foil dimensions, minimum clearance, and air viscosity at the operating temperature. To prevent failure by TEI, the system of bearing must implement effective thermal management. Based on the rotational speed, FBs produces heat because of viscous shear. The generated heat could cause hotspots locally, resulting in an additional thermal gradient, and hence seizure of bearing would occur. In a study, Heshmat et al. [139] acknowledged the importance of adapting the compliant FB in the engine of a turbojet that functioned at a rotation speed, with the bearing temperature as 60,000 rpm and 650 °C, respectively. They calculated the minimum flow of air necessary for a certain speed. When the rotor's speed reached 60,000 rpm, they observed that the feed rate of airflow should be 566 L/min. The bearing temperature was destabilized and increased continuously without balancing for a cooling airflow rate under 140 L/min. They also formulated a comprehensive thermal mapping to evaluate the thermal gradients of FB axially in a test rig in which the rotors engine was assisted by REB and FB at the ends of the turbine and compressor, respectively. They acknowledged that a minimum rate of flow results in FBs greater temperatures with minimized thermal gradient and without affecting the engine's compressor's efficiency.

3.3 Critical inferences for the thermo-mechanical analysis of the TC rotor system:

- In a turbocharger rotor system, the shear power generated can enhance by an excellent supply of pressure, lower oil temperatures, or greater clearances. In addition, the provision of additional grooves axially on the interior side of SFRB can improve the dynamic stability and increment in the flow of drawn oil and heat and drag power from the journal.
- The stability of the bearing, loss of energy, and load capacity relied on the speed of the ring. Therefore, the effects due to thermal conditions could influence the FRB's performance as well as the reduction of ring speed.
- For greater amplitudes, the variation in the rotor's and ring's temperatures can influence the change in the oil film's thermal expansion and the clearances.
- With the vital flow of heat into the interior film from the journal across all the shaft speeds, the lubricant's streams can carry greater than 70% of thermal energy from the input of total energy, and the remaining can conduct via the casing of the turbocharger. This distribution of thermal energy can justify by feeding a sufficient flow of lubricant to the bearing system.
- In the case of FRBs, the temperature of the ring will vary in all directions. Mainly in the axial direction due to the heat conduction from TB into the ring. The total energy flow equals the viscous drag power losses from the inner film in the radial bearing and the thrust bearing plus the heat soaked from the shaft.

4 Conclusions

This review paper reports a summarized literature survey performed over the past thirty years on the characteristics of turbochargers supported on Journal bearings, ball bearings, floating ring bearings and gas foil bearings. A complex relationship is observed between the theoretical and analytical concepts. Various analyses, including stability, dynamic, and thermo-mechanical type are presented in detail for the turbocharger rotor system. The significant findings were listed below.

- Optimizing and redesigning the mass distribution of the TC rotor can be an alternative approach to improve dynamic performance. However, the lower and higher load parameters can cause supercritical and subcritical bifurcations. That's why choosing the load parameter (σ) as low as feasible is advisable. Increased lubricant viscosity leads to higher fluid pressure, and bearing clearance affects the exterior film pressure distribution. As a result, the journal bearing can lose its stability either at the super- or subcritical bifurcation.
- The frequencies generated in a TC due to interior and exterior oil films whirling and whipping nature will induce the gyroscopic forward modes, which were conical and translational in shape.
- The staggered bumps configuration in aerodynamic foil journal bearings generates increased rigidity with increasing load and improved stability at incredible speeds. FRGBs stability performance can be enhanced by greater lower values of eccentricity as well as mass ratio, zero or negative values of speed ratio and increment in the pressure of supply gas at a medium or more excellent range of speeds. In addition, three pad bearings with variable stiffness gradients show excellent qualities of whirl stability.
- An increment in the oil inlet temperature can decrease interior and exterior oil film viscosities, the vibrational amplitude of interior oil film, consumption of frictional power, and the rise of temperature. Therefore, a combination of whirl and whip with interior and exterior oil films amplitude of vibration can result in a minimum vibration level in the TC rotor system. In addition, the whirl of exterior oil film and whip of interior oil film can influence the system's stability, which is caused by the increment in the oil inlet temperature.
- The frequency and amplitude of shaft vibrations characterize an oil whirl. The oil supply pressure can restrict the magnitude of the oil whirl. An increment in the speed can lead to the emergence of an oil whirl, which further leads to rotor failure. The rotor system's instabilities can be dominated by the whirl of oil caused by a minimal clearance ratio. Conversely, oil whirl in the outer region dominates the instability regions with large clearance ratios.
- The dry friction generated inside can influence the foil structure's dynamic behaviors. Compared with the rigid-type bearings, the stability characteristics of bearings with a compliant surface can enhance due to the deflection of the structure. Introducing friction and

unbalance can improve stability by doubling and carrying out unbalanced mass with greater magnitude. GFB with metal shims can result in more excellent stability and performance efficiently.

- An increment in the stability can be possible by the increment of FAB length-to-radius ratio, increment in the compliance of foil structure, and reduction of radial clearance, which is undeformed. Furthermore, an increment in the lift-off speed and the stiffness of FB structure can be possible by the coefficient of friction for the sleeve of the bearing. At elevated temperatures, the performance of FB is satisfactory and can accommodate considerable temperature gradients.
- In the case of journal bearings, the surface roughness patterns along the transverse and longitudinal directions could enhance and reduce system stability. Meanwhile, in the case of REBs, decrement in the amplitude levels of vibration could be possible by applying initial preload axially.
- In the case of FTB, an increment in the static load and a decrement in the displacement amplitude dynamically can enhance the structure's stiffness with non-variable damping. Adapting a coating with a significant coefficient of friction, lubricant-coated surfaces, increment in the thickness of foil bump, and proper selection of pivot center location can result in dynamic damping and stiffness of the structure. Similarly, an increment in the ratio of eccentricity and bearing number or a decrement in inclined parts gradient can enhance the torque of the bearing and the load. Furthermore, for a particular speed range, an increment in the external radius and speed of rotation of TB can improve the load capacity at the maximum level.

5 Future scope

- Innovative bearing bore configurations must design to guarantee stability throughout the complete operating range of speed. Also, the origin of the energy that causes the instability must be investigated. Also, it is essential to examine the bearing's bifurcation properties for L/D ratio greater than 0.5 because for larger eccentricity values, a subcritical domain predicted by the theoretical studies implies that working under heavy load conditions leads to instability in the bearing.
- In the case of a multi-disk rotor, the impacts of the disk mass location concerning nonlinearity sources, the consequences of its flexibility, and unbalance of bifurcation features still need to investigate.
- The combined influences of clearances and the temperature-dependent viscosity in the transient regime on the overall system dynamics still need investigation.

Appendix 1: Summary of important research performed on the turbocharger rotor supported on the rolling element, oil film and oil-free bearings

Focus area	Type of bearing	Methodology	Ref	Key findings
Stability analysis	Floating ring bearings	FEM-based TC model applied with unbalance, nonlinear time transient response	[12]	Instability at the compressor end, reduction in subsynchronous vibration
Dynamic analysis	Floating ring bearings	FEM-based TC model applied with rotating unbalance and engine excitations	[16]	Reduced sub-synchronous vibrations at high speeds due to the force of inertia
Stability analysis	Floating ring bearings	Hopf's bifurcation theory, whirl orbits	[21]	Occurrence of super- and subcritical bifurcations
Stability analysis	Floating ring bearings	FEM-based TC model applied with cascade spectrum	[22] [23]	Multiple regimes of vibration by the oil-lubricated bearings, the transformation of whirl into a whip

Focus area	Type of bearing	Methodology	Ref	Key findings
Stability analysis	Floating ring bearings	FEM-based continuum model with direct integration methods and mode superposition schemes	[25] [26]	Failure of the system due to oil whip
Stability analysis	Floating ring bearings	FEM-based TC model applied with unbalance, run-up and run-down simulations	[27]	Increment in the instability threshold due to the increment of the moment of unbalance
Stability analysis	Full floating ring bearings	FEM-based Jeffcott rotor with the run-up and run-down simulations	[28]	Total Instability
Stability analysis	Floating ring bearings	FEM model with numerical continuation approach	[31] [32]	The source of the steady-state instability and the emergence of critical limit cycles
Dynamic analysis	Floating ring bearings	A FEM-based model analyzed by numerical continuation approach. Journal speed as a parametric study	[33]	The bearing modulus plays a crucial role in evaluating the threshold speed of rotor stability and sequences of bifurcation
Dynamic analysis	Floating ring bearings	Hopf bifurcation theory	[34]	Identification of the presence and size of the stable and unstable limit cycles
Dynamic analysis	Floating ring bearings	A FEM-based model operated at transient conditions	[38]	Angular acceleration and deceleration have negligible influence on the system's total stability
Stability analysis	Floating ring bearings	FEM model with a threshold value of 0.5 and waterfall diagrams	[44]	gyroscopic effects on the conical whirl instability of a turbocharger
Dynamic analysis	Floating ring bearings + Thrust bearings	A FEM-based model with Newmark algorithm for time integration	[45] [46]	Influences of thrust bearing on the lateral dynamics of Turbochargers
Dynamic analysis	Cylindrical Floating ring bearings	The modified particle swarm optimization (MPSO) scheme	[140]	Prediction of bearing coefficients
Dynamic analysis	Aerodynamic (gas) bearings	A nonlinear time-dependent calculation is used for the dynamic simulation of a rotor	[57]	Additional damping can enhance stability
Dynamic analysis	Gas foil bearings	Stationary and nonlinear Stability analysis	[59]	Compliant surface bearings can have better stability characteristics than rigid bearings

Focus area	Type of bearing	Methodology	Ref	Key findings
Dynamic analysis	Gas foil bearings	Coulomb damping with a nonlinear transient analysis approach	[61]	FB is much more effective at the resonance condition for controlling vibration amplitude
Stability analysis	Gas foil bearings	Analysis by an experimental test setup with three uniform metal shims	[66]	An improved LCC and stability with reduced amplitude of vibration
Dynamic analysis	Airfoil bearings	Evaluation of the elastic structure's dynamic stiffness and damping by Dynamic shaker tests with a harmonic excitation	[69] [70] [69]	Influences of introducing metal shims between the bumps and the bearing sleeve
Dynamic analysis	Foil thrust bearings	Experimental tests with various static loads and frequency of excitations	[76]	Enhanced stiffness and decreased damping
Elasto-gas-dynamic analysis	Airfoil thrust bearings	A Reissner–Mindlin-type shell theory models the exact geometry of the bump foil	[77]	AFTB possess minimized load capacity than rigid types
Dynamic analysis	Viscoelastic supports	The hybrid model incorporated oil and Viscoelastic supports	[86]	Minimized unbalanced amplitude response
Dynamic Analysis	Rolling bearings	Increasing the number of balls	[97]	Enhanced Stiffness of system
Thermo-mechanical analysis	Semi-floating ring bearings	Various parametric studies, along with the coupled Reynolds and the thermal energy transport equations, for the solution of the pressure and temperature zones of the interior and exterior films	[108]	Additional grooves axially on the interior side of SFRB can improve the dynamic stability and increment the flow of drawn oil and heat and drag power from the journal
Thermo-mechanical analysis	Floating ring bearings	A FEM-based model with CHT numerical simulation	[110]	Importance of predicting the dissipation of damped internal energy in the temperature zone for better rotor dynamic characteristics
Thermo-mechanical analysis	Floating ring bearings	Integration of thermal flow model with nonlinear rotor dynamics	[114]	Emerge of aerodynamic loads and increment in the journal speed

Focus area	Type of bearing	Methodology	Ref	Key findings
Thermo-mechanical analysis	Floating ring bearings	Simulation and experimental studies of 3D THD model integrated with Downsons and transient 3D thermal equation	[116]	Existence of sub-synchronous frequencies under excitation
Thermo-mechanical analysis	Bump-type gas foil bearings	2D THD bulk flow with lump parameter thermal model	[120]	Reduced coefficients of heat transfer
Thermo-mechanical analysis	Air foil thrust bearings	A FEM-based 3D TEHD model integrated with the Reynolds equation, 3D energy equation	[125]	An increment in the speed can enhance the AFTBs load capacity up to a certain critical speed
Thermal analysis	Foil air bearings	An experimental analysis by measuring friction and wear data for coated surfaces	[128]	Thick solid hard coating on the journal surface is effective for better performance
Thermal analysis	Gas foil bearings	Experiments with high-temperature FB	[134] [135] [136]	High temperature leads to seizure which the vibration signal of the rotor could not detect
Thermal analysis	Bump-type foil bearings	Analytical model of thermoelastic instability (TEI)	[138]	Evaluate critical speed for TEI using perturbed heat waves
Thermal analysis	Air foil bearings	Forced air cooling method	[139]	Find optimum cooling flow and double bump strip layer to be more effective for cooling

Appendix 2: The detailed formulation for full and semi-floating ring bearings

The terminology involved in the analytical formulations from Eq. (1–12) is listed as follows:

$$\begin{aligned} \mathrm{x_j} &= \mathrm{X_j} - \mathrm{X_r}; \\ \mathrm{y_j} &= \mathrm{Y_j} - \mathrm{Y_r}; \\ \dot{x}_j &= \dot{X}_j - \dot{X}_r; \\ \dot{y}_j &= \dot{Y}_j - \dot{Y}_r \end{aligned} \tag{33}$$

With the assumption of iso-viscous Newtonian lubricating oil and the infinite short-bearing theory, the analytical solution of Reynolds Eqs. (1) and (2) can be obtained as follows:

$$\frac{\partial}{\partial Z_i}\left(\frac{h_i^3}{12\mu_i}\frac{\partial p_\mathrm{i}}{\partial Z_i}\right) = \frac{\Omega_j + \Omega_r}{2}\frac{\partial h_\mathrm{i}}{\partial \theta_i} + \frac{\partial h_\mathrm{i}}{\partial t} \tag{34}$$

$$\frac{\partial}{\partial Z_o}\left(\frac{h_o^3}{12\mu_o}\frac{\partial p_\mathrm{o}}{\partial Z_o}\right) = \frac{\Omega_r}{2}\frac{\partial h_\mathrm{o}}{\partial \theta_i} + \frac{\partial h_\mathrm{o}}{\partial t} \tag{35}$$

The iso-viscous Newtonian lubricating oil assumption is applied to both films, and the boundary conditions are given as follows:

$$p_\mathrm{i}\left(\theta_i, Z_\mathrm{i} = -\frac{L_i}{2}\right) = p_i\left(\theta_i, Z_\mathrm{i} = +\frac{L_i}{2}\right) = 0 \tag{36}$$

$$p_\mathrm{o}\left(\theta_o, Z_\mathrm{o} = -\frac{L_i}{2}\right) = p_o\left(\theta_o, Z_\mathrm{o} = +\frac{L_o}{2}\right) = 0 \tag{37}$$

For the numerical calculation, the introduction of dimensionless variables is given as follows:

$$\begin{aligned}&\overline{x}_j=\frac{x_j}{C_1},\overline{y}_j=\frac{y_j}{C_1},\overline{z}_i=\frac{Z_i}{L_i},\overline{x}_j'=\frac{\dot{x}_j}{C_1\left(\Omega_j+\Omega_r\right)},\overline{y}_j'=\frac{\dot{y}_j}{C_1\left(\Omega_j+\Omega_r\right)},\\&\overline{p}_i=\frac{p_i}{6\mu_i\left(\Omega_j+\Omega_r\right)\left(R_i/C_1\right)^2};\overline{x}_r=\frac{X_r}{C_2};\overline{y}_r=\frac{Y_r}{C_2};\overline{z}_o=\frac{Z_o}{L_o};\overline{x}_r'=\frac{\dot{X}_r}{C_2\Omega_r};\overline{y}_r'=\frac{\dot{Y}_r}{C_2\Omega_r}\\&\overline{p}_o=\frac{p_o}{6\mu_o\Omega_r\left(R_{ro}/C_2\right)^2}\end{aligned}\tag{38}$$

$$\overline{p}_i=\frac{1}{2}\frac{L_i^2}{D_j^2}\frac{\left(4\overline{z}_i^2-1\right)\left[\left(\overline{x}_j-2\overline{y}_j'\right)\sin\theta_i-\left(\overline{y}_j+2\overline{x}_j'\right)\cos\theta_i\right]}{\left(1-\overline{x}_j\cos\theta_i-\overline{y}_j\sin\theta_i\right)^3}\tag{39}$$

$$\overline{p}_o=\frac{1}{2}\frac{L_o^2}{D_{ro}^2}\frac{\left(4\overline{z}_o^2-1\right)\left[\left(\overline{x}_r-2\overline{y}_r'\right)\sin\theta_o-\left(\overline{y}_r+2\overline{x}_r'\right)\cos\theta_o\right]}{\left(1-\overline{x}_r\cos\theta_o-\overline{y}_r\sin\theta_o\right)^3}\tag{40}$$

The conditions to develop the oil film force located at the intervals $\left(\alpha_i,\alpha_i+\pi\right)$ and $\left(\alpha_o,\alpha_o+\pi\right)$ are provided as follows:

$$\overline{p}_i\left(\alpha_i\right)=0,\ \frac{\partial\overline{p}_i}{\partial\theta_i}\Big|\theta_i=\alpha_i>0;\overline{p}_o\left(\alpha_o\right)=0,\ \frac{\partial\overline{p}_o}{\partial\theta_o}\Big|\theta_o=\alpha_o>0\tag{41}$$

the angles α_i and α_o can be described as

$$\alpha_i=-\operatorname{sgn}\left(\overline{y}_j+2\overline{x}_j'\right)\cos^{-1}\left(-\frac{\overline{x}_j-2\overline{y}_j'}{\sqrt{\left(\overline{y}_j+2\overline{x}_j'\right)^2+\left(\overline{x}_j-2\overline{y}_j'\right)^2}}\right)\tag{42}$$

$$\alpha_o=-\operatorname{sgn}\left(\overline{y}_r+2\overline{x}_r'\right)\cos^{-1}\left(-\frac{\overline{x}_r-2\overline{y}_r'}{\sqrt{\left(\overline{y}_r+2\overline{x}_r'\right)^2+\left(\overline{x}_r-2\overline{y}_r'\right)^2}}\right)\tag{43}$$

$$G_i\left(\overline{x}_j,\overline{y}_j,\alpha_i\right)=\frac{2}{\sqrt{1-\overline{x}_j^2-\overline{y}_j^2}}\left[\frac{\pi}{2}+\tan^{-1}\left(\frac{\overline{y}_j\cos\alpha_i-\overline{x}_j\sin\alpha_i}{\sqrt{1-\overline{x}_j^2-\overline{y}_j^2}}\right)\right]\tag{44}$$

$$V_i\left(\overline{x}_j,\overline{y}_j,\alpha_i\right)=\frac{2+\left(\overline{y}_j\cos\alpha_i-\overline{x}_j\sin\alpha_i\right)G_i\left(\overline{x}_j,\overline{y}_j,\alpha_i\right)}{\left(1-\overline{x}_j^2-\overline{y}_j^2\right)}\tag{45}$$

$$S_i\left(\overline{x}_j,\overline{y}_j,\alpha_i\right)=\frac{\overline{x}_j\cos\alpha_i+\overline{y}_j\sin\alpha_i}{1-\left(\overline{x}_j\cos\alpha_i+\overline{y}_j\sin\alpha_i\right)^2}.\tag{46}$$

$$G_o\left(\overline{x}_r,\overline{y}_r,\alpha_o\right)=\frac{2}{\sqrt{1-\overline{x}_r^2-\overline{y}_r^2}}\left[\frac{\pi}{2}+\tan^{-1}\left(\frac{\overline{y}_r\cos\alpha_o-\overline{x}_r\sin\alpha_o}{\sqrt{1-\overline{x}_r^2-\overline{y}_r^2}}\right)\right]\tag{47}$$

$$V_o\left(\overline{x}_r,\overline{y}_r,\alpha_o\right)=\frac{2+\left(\overline{y}_r\cos\alpha_o-\overline{x}_r\sin\alpha_o\right)G_o\left(\overline{x}_r,\overline{y}_r,\alpha_o\right)}{\left(1-\overline{x}_r^2-\overline{y}_r^2\right)}\tag{48}$$

$$S_o\left(\overline{x}_r,\overline{y}_r,\alpha_o\right)=\frac{\overline{x}_r\cos\alpha_o+\overline{y}_r\sin\alpha_0}{1-\left(\overline{x}_r\cos\alpha_o+\overline{y}_r\sin\alpha_0\right)^2}\tag{49}$$

In the case of semi-floating ring bearings

The bulk-flow thermal energy transport equation for the inner film at a temrature T_i is (from Eq. 23)

$$\dot{m}_{\theta_i}=(\rho Uh)_i=-\frac{\rho h_i^3}{12\mu_i}\frac{\partial p_i}{R_j\partial\theta}+(\rho h)_i\frac{1}{2}U_s\tag{50}$$

$$\dot{m}_{z_i}=(\rho Wh)_i=-\frac{\rho h_i^3}{12\mu_i}\frac{\partial p_i}{R_j\partial z_I}\tag{51}$$

with

$$U_s=R_j\Omega_s\tag{52}$$

The shear mechanical energy dissipation function (Φ_i) is:

$$\Phi_i=12\frac{\mu_i}{h_i}\left[W_i^2+\frac{1}{12}U_s^2+\left(U_i-\frac{1}{2}U_s\right)^2\right]\tag{53}$$

The mean flow velocities in the circumferential and axial directions are,

$$U_i=-\frac{h_i^2}{12\mu_i}\frac{\partial p_i}{R_j\partial\theta}+\frac{U_s}{2},W_i=-\frac{h_i^2}{12\mu_i}\frac{\partial p_i}{\partial z_i}\tag{54}$$

The bulk-flow thermal energy transport equation for the outer film at a temperature T_o is (from Eq. 24)

$$\dot{m}_{\theta_o} = (\rho U h)_o = -\frac{\rho h_o^3}{12\mu_o}\frac{\partial p_o}{R_o \partial \theta} \tag{55}$$

$$\dot{m}_{z_o} = (\rho W h)_o = -\frac{\rho h_o^3}{12\mu_o}\frac{\partial p_o}{\partial z_o} \tag{56}$$

$$\Phi_o = 12\frac{\mu_o}{h_o}\left[W_o^2 + U_o^2\right] \tag{57}$$

with the mean flow velocities as:

$$U_o = -\frac{h_{\mathrm{o}}^2}{12\mu_{\mathrm{o}}}\frac{\partial p_{\mathrm{o}}}{R_{\mathrm{o}}\partial\theta}, W_o = -\frac{h_{\mathrm{o}}^2}{12\mu_o}\frac{\partial p_{\mathrm{o}}}{\partial z_o} \tag{58}$$

Acknowledgements The authors would like to thank Vellore Institute of Technology, Vellore, Tamil Nadu, India, for providing research facilities.

Funding There is no funding for the above research work.

Declarations

Conflict of interest The authors declare that they have no conflict of interest.

References

1. Peixoto TF, Cavalca KL (2022) A review on the rotor dynamics of automotive turbochargers. In: Parikyan T (ed) Advances in engine and powertrain research and technology. Mechanisms and machine science. Springer International Publishing, Cham, pp 97–126
2. Kirk RG, Alsaeed AA, Gunter EJ (2007) Stability analysis of a high-speed automotive turbocharger. Tribol Trans 50:427–434. https://doi.org/10.1080/10402000701476908
3. Ashtekar A, Tian L, Lancaster C (2014) An analytical investigation of turbocharger rotor-bearing dynamics with rolling element bearings and squeeze film dampers. In: Institute of mechanical engineers (ed) 11th international conference on turbochargers and turbocharging. Woodhead Publishing, Oxford, pp 361–373. https://doi.org/10.1533/978081000342.361
4. Khonsari M (2021) Air bearings theory, design and applications. J Tribol 143:116501. https://doi.org/10.1115/1.4051155
5. Boyaci A, Lu D, Schweizer B (2015) Stability and bifurcation phenomena of Laval/Jeffcott rotors in semi-floating ring bearings. Nonlinear Dyn 79:1535–1561. https://doi.org/10.1007/s11071-014-1759-5
6. Tian L, Wang WJ, Peng ZJ (2011) Dynamic behaviours of a full floating ring bearing supported turbocharger rotor with engine excitation. J Sound Vib 330:4851–4874. https://doi.org/10.1016/j.jsv.2011.04.031
7. Nguyen-Schäfer H (2012) Rotordynamics of automotive turbochargers. Springer Berlin Heidelberg, Berlin
8. Bonneau D, Fatu A, Souchet D (2014) Hydrodynamic bearings: bonneau/hydrodynamic bearings. John Wiley & Sons Inc, Hoboken
9. Holt C, San Andreś L, Sahay S et al (2005) Test response and nonlinear analysis of a turbocharger supported on floating ring bearings. J Vib Acoust 127:107–115. https://doi.org/10.1115/1.1857922
10. Dyk Š, Smolík L, Rendl J (2020) Predictive capability of various linearization approaches for floating-ring bearings in nonlinear dynamics of turbochargers. Mech Mach Theory 149:103843. https://doi.org/10.1016/j.mechmachtheory.2020.103843
11. Knoll G, Seemann W, Proppe C et al (2010) Run-up of turbocharger rotors in nonlinearly modelled floating bush bearings. MTZ Worldw 71:50–55. https://doi.org/10.1007/BF03227992
12. Gordon Kirk R, Alsaeed AA (2011) Induced unbalance as a method for improving the dynamic stability of high-speed turbochargers. Int J Rotat Mach 2011:952869. https://doi.org/10.1155/2011/952869
13. Zhang H, Shi ZQ, Zhen D, et al (2012) Stability analysis of a turbocharger rotor system supported on floating ring bearings. In: Journal of physics: conference series 364:012032. https://doi.org/10.1088/1742-6596/364/1/012032
14. Jones DA (1993) Short journal bearing lubrication theory. Tribol Ser 26:1–14. https://doi.org/10.1016/S0167-8922(08)70005-1
15. Bin G-F, Huang Y, Guo S-P et al (2018) Investigation of induced unbalance magnitude on dynamic characteristics of high-speed turbocharger with floating ring bearings. Chin J Mech Eng 31:88. https://doi.org/10.1186/s10033-018-0287-5
16. Singh A, Gupta TC (2020) Effect of rotating unbalance and engine excitations on the nonlinear dynamic response of turbocharger flexible rotor system supported on floating ring bearings. Arch Appl Mech 90:1117–1134. https://doi.org/10.1007/s00419-020-01660-z
17. Woschke E, Daniel C, Nitzschke S (2017) Excitation mechanisms of non-linear rotor systems with floating ring bearings-simulation and validation. Int J Mech Sci 134:15–27. https://doi.org/10.1016/j.ijmecsci.2017.09.038
18. Ziese C, Irmscher C, Nitzschke S et al (2021) Run-up simulation of a semi-floating ring supported turbocharger rotor considering thrust bearing and mass-conserving cavitation. Lubricants 9:44. https://doi.org/10.3390/lubricants9040044
19. Hori Y (1959) A theory of oil whip. J Appl Mech 26:189–198. https://doi.org/10.1115/1.4011981
20. Muszynska A (2005) Rotordynamics. CRC Press
21. Myers CJ (1984) Bifurcation theory applied to oil whirl in plain cylindrical journal bearings. J Appl Mech 51:244–250. https://doi.org/10.1115/1.3167607
22. Sheng Chen G, Liu X (2016) Friction dynamics and diagnosis of rotor systems. In: Friction dynamics. Elsevier, pp 247–298. 10.1016/B978-0-08-100285-8.00006–7
23. Muszynska A (1986) Whirl and whip—rotor/bearing stability problems. J Sound Vib 110:443–462. https://doi.org/10.1016/S0022-460X(86)80146-8
24. Muszynska A (1988) Stability of whirl and whip in rotor/bearing systems. J Sound Vib 127:49–64. https://doi.org/10.1016/0022-460X(88)90349-5
25. Shaw J, Shaw SW (1990) The effects of unbalance on oil whirl. Nonlinear Dyn 1:293–311. https://doi.org/10.1007/BF01865277
26. JianPing J, Guang M, Yi S, SongBo X (2004) On the nonlinear dynamic behavior of a rotor–bearing system. J Sound Vib 274:1031–1044. https://doi.org/10.1016/S0022-460X(03)00663-1
27. Jing J, Meng G, Sun Y, Xia S (2005) On the oil-whipping of a rotor-bearing system by a continuum model. Appl Math Model 29:461–475. https://doi.org/10.1016/j.apm.2004.09.003
28. de Castro HF, Cavalca KL, Nordmann R (2008) Whirl and whip instabilities in rotor-bearing system considering a nonlinear force model. J Sound Vib 317:273–293. https://doi.org/10.1016/j.jsv.2008.02.047
29. Schweizer B (2009) Oil whirl, oil whip and whirl/whip synchronization occurring in rotor systems with full-floating ring

bearings. Nonlinear Dyn 57:509–532. https://doi.org/10.1007/s11071-009-9466-3
30. Kirk RG, Alsaeed A, Liptrap J et al (2008) Experimental test results for vibration of a high speed diesel engine turbocharger. Tribol Trans 51:422–427. https://doi.org/10.1080/10402000801911853
31. Schweizer B (2010) Dynamics and stability of turbocharger rotors. Arch Appl Mech 80:1017–1043. https://doi.org/10.1007/s00419-009-0331-0
32. Boyaci A, Hetzler H, Seemann W et al (2009) Analytical bifurcation analysis of a rotor supported by floating ring bearings. Nonlinear Dyn 57:497–507. https://doi.org/10.1007/s11071-008-9403-x
33. Boyaci A, Seemann W, Proppe C (2010) Stability and bifurcations of rotors in fluid film bearings. Proc Appl Math Mech 10:235–236. https://doi.org/10.1002/pamm.201010110
34. Amamou A (2021) Nonlinear stability analysis and numerical continuation of bifurcations of a rotor supported by floating ring bearings. Proc Inst Mech Eng Part C J Mech Eng Sci. https://doi.org/10.1177/09544062211026340
35. Amamou A, Chouchane M (2011) Non-linear stability analysis of floating ring bearings using Hopf bifurcation theory. Proc Inst Mech Eng C J Mech Eng Sci 225:2804–2818. https://doi.org/10.1177/0954406211413520
36. Gunter EJ, Wang WJ (2005) Dynamic analysis of a turbocharger in floating bushing bearings. ISCORMA-3, Dyrobes 19:23
37. Bonello P (2009) Transient modal analysis of the non-linear dynamics of a turbocharger on floating ring bearings. Proc Inst Mech Eng Part J J Eng Tribol 223:79–93. https://doi.org/10.1243/13506501JET436
38. Schweizer B (2009) Total instability of turbocharger rotors—physical explanation of the dynamic failure of rotors with full-floating ring bearings. J Sound Vib 328:156–190. https://doi.org/10.1016/j.jsv.2009.03.028
39. Mutra RR, Srinivas J (2020) Dynamic analysis of a turbocharger rotor-bearing system in transient operating regimes. J Inst Eng India Ser C 101:771–783. https://doi.org/10.1007/s40032-020-00591-6
40. Tian L, Wang WJ, Peng ZJ (2012) Effects of bearing outer clearance on the dynamic behaviours of the full floating ring bearing supported turbocharger rotor. Mech Syst Signal Process 31:155–175. https://doi.org/10.1016/j.ymssp.2012.03.017
41. Tian L, Wang WJ, Peng ZJ (2013) Nonlinear effects of unbalance in the rotor-floating ring bearing system of turbochargers. Mech Syst Signal Process 34:298–320. https://doi.org/10.1016/j.ymssp.2012.07.017
42. Liang F, Zhou M, Xu Q (2016) Effects of semi-floating ring bearing outer clearance on the subsynchronous oscillation of turbocharger rotor. Chin J Mech Eng 29:901–910. https://doi.org/10.3901/CJME.2016.0421.057
43. Mutra RR, Srinivas J (2021) Parametric design of turbocharger rotor system under exhaust emission loads via surrogate model. J Braz Soc Mech Sci Eng 43:117. https://doi.org/10.1007/s40430-021-02809-9
44. Tamunodukobipi D, Ho Kim C, Lee Y-B (2015) Dynamic performance characteristics of floating-ring bearings with varied oil-injection swirl-control angles. J Dyn Syst Measurement Control 137:021002. https://doi.org/10.1115/1.4027912
45. Kamesh P, Brennan MJ, Holmes R (2012) On the stabilising effect of gyroscopic moments in an automotive turbocharger. Proc Inst Mech Eng C J Mech Eng Sci 226:2485–2495. https://doi.org/10.1177/0954406212438142
46. Peixoto TF, Cavalca KL (2020) Thrust bearing coupling effects on the lateral dynamics of turbochargers. Tribol Int 145:106166. https://doi.org/10.1016/j.triboint.2020.106166
47. Peixoto TF, Nordmann R, Cavalca KL (2021) Dynamic analysis of turbochargers with thermo-hydrodynamic lubrication bearings: abstract. J Sound Vib 505:116140
48. Mutra RR, Srinivas J, Singh D (2020) Thrust bearing influence on the stability analysis of turbocharger rotor-bearing system. In: Popov I, Rossikhin Yu A, Shitikova MV (eds) Advances in rotor dynamics, control, and structural health monitoring. Springer, Singapore, pp 85–98
49. Peixoto TF, Cavalca KL (2019) Investigation on the angular displacements influence and nonlinear effects on thrust bearing dynamics. Tribol Int 131:554–566. https://doi.org/10.1016/j.triboint.2018.11.019
50. Tanaka M, Hori Y (1972) Stability characteristics of floating bush bearings. J Lubr Technol 94:248–256. https://doi.org/10.1115/1.3451700
51. Lee Y-B, Park D-J, Sim K (2015) Rotordynamic performance measurements of an oil-free turbocharger supported on gas foil bearings and their comparisons to floating ring bearings. Int J Fluid Mach Syst 8:23–35. https://doi.org/10.5293/IJFMS.2015.8.1.023
52. Kim D, Lee AS, Choi BS (2014) Evaluation of foil bearing performance and nonlinear rotordynamics of 120 kW oil-free gas turbine generator. J Eng Gas Turbines Power 136:032504. https://doi.org/10.1115/1.4025898
53. Hassini MA, Arghir M (2012) A simplified nonlinear transient analysis method for gas bearings. J Tribol 134:011704. https://doi.org/10.1115/1.4005772
54. Bhore SP, Darpe AK (2013) Nonlinear dynamics of flexible rotor supported on the gas foil journal bearings. J Sound Vib 332:5135–5150. https://doi.org/10.1016/j.jsv.2013.04.023
55. Bonello P, Pham HM (2014) The efficient computation of the nonlinear dynamic response of a foil–air bearing rotor system. J Sound Vib 333:3459–3478. https://doi.org/10.1016/j.jsv.2014.03.001
56. Bonello P, Pham HM (2014) Nonlinear dynamic analysis of high speed oil-free turbomachinery with focus on stability and self-excited vibration. J Tribol 136:041705. https://doi.org/10.1115/1.4027859
57. Gu Y, Ren G, Zhou M (2020) A fully coupled elastohydrodynamic model for static performance analysis of gas foil bearings. Tribol Int 147:106297. https://doi.org/10.1016/j.triboint.2020.106297
58. Bou-Saïd B, Grau G, Iordanoff I (2008) On nonlinear rotor dynamic effects of aerodynamic bearings with simple flexible rotors. J Eng Gas Turbines Power 130:012503. https://doi.org/10.1115/1.2747262
59. Zywica G, Baginski P, Bogulicz M (2021) Experimental and numerical evaluation of the damping properties of a foil bearing structure taking into account the static and kinetic dry friction. J Braz Soc Mech Sci Eng 43:7. https://doi.org/10.1007/s40430-020-02720-9
60. Le Lez S, Arghir M, Frêne J (2009) Nonlinear numerical prediction of gas foil bearing stability and unbalanced response. J Eng Gas Turbines Power 131:012503. https://doi.org/10.1115/1.2967481
61. Fangcheng X, Daejong K (2016) Dynamic performance of foil bearings with a quadratic stiffness model. Neurocomputing 216:666–671. https://doi.org/10.1016/j.neucom.2016.08.019
62. Lee D-H, Kim Y-C, Kim K-W (2009) The dynamic performance analysis of foil journal bearings considering coulomb friction: rotating unbalance response. Tribol Trans 52:146–156. https://doi.org/10.1080/10402000802192685
63. Zywica G, Baginski P, Bogulicz M et al (2022) Numerical identification of the dynamic characteristics of a nonlinear foil bearing structure: effect of the excitation force amplitude and

the assembly preload. J Sound Vib 520:116663. https://doi.org/10.1016/j.jsv.2021.116663
64. Balducchi F, Arghir M, Gauthier R (2015) Experimental analysis of the unbalance response of rigid rotors supported on aerodynamic foil bearings. J Vib Acoust 137:061014. https://doi.org/10.1115/1.4031409
65. Larsen JS, Santos IF (2015) On the nonlinear steady-state response of rigid rotors supported by air foil bearings—theory and experiments. J Sound Vib 346:284–297. https://doi.org/10.1016/j.jsv.2015.02.017
66. von Osmanski S, Larsen JS, Santos IF (2017) A fully coupled air foil bearing model considering friction–theory & experiment. J Sound Vib 400:660–679. https://doi.org/10.1016/j.jsv.2017.04.008
67. Kim TH, Andrés LS (2009) Effects of a mechanical preload on the dynamic force response of gas foil bearings: measurements and model predictions. Tribol Trans 52:569–580. https://doi.org/10.1080/10402000902825721
68. Schiffmann J, Spakovszky ZS (2013) Foil bearing design guidelines for improved stability. J Tribol 135:011103. https://doi.org/10.1115/1.4007759
69. Andrés LS, Kim TH (2008) Forced nonlinear response of gas foil bearing supported rotors. Tribol Int 41:704–715. https://doi.org/10.1016/j.triboint.2007.12.009
70. Hoffmann R, Liebich R (2017) Experimental and numerical analysis of the dynamic behaviour of a foil bearing structure affected by metal shims. Tribol Int 115:378–388. https://doi.org/10.1016/j.triboint.2017.04.040
71. Hoffmann R, Liebich R (2018) Characterisation and calculation of nonlinear vibrations in gas foil bearing systems–an experimental and numerical investigation. J Sound Vib 412:389–409. https://doi.org/10.1016/j.jsv.2017.09.040
72. Heshmat H, Walowit JA, Pinkus O (1983) Analysis of gas lubricated compliant thrust bearings. J Lubr Technol 105:638–646. https://doi.org/10.1115/1.3254696
73. Ku C-PR (1994) Dynamic structural properties of compliant foil thrust bearings—comparison between experimental and theoretical results. J Tribol 116:70–75. https://doi.org/10.1115/1.2927049
74. Feng K, Liu L-J, Guo Z-Y, Zhao X-Y (2016) Parametric study on static and dynamic characteristics of bump-type gas foil thrust bearing for oil-free turbomachinery. Proc Inst Mech Eng Part J J Eng Tribol 230:944–961. https://doi.org/10.1177/1350650115621015
75. Park D-J, Kim C-H, Jang G-H, Lee Y-B (2008) Theoretical considerations of static and dynamic characteristics of air foil thrust bearing with tilt and slip flow. Tribol Int 41:282–295. https://doi.org/10.1016/j.triboint.2007.08.001
76. Zhou Q, Hou Y, Chen C (2009) Dynamic stability experiments of compliant foil thrust bearing with viscoelastic support. Tribol Int 42:662–665. https://doi.org/10.1016/j.triboint.2008.09.005
77. Balducchi F, Arghir M, Gauthier R (2015) Experimental analysis of the dynamic characteristics of a foil thrust bearing. J Tribol 137:021703. https://doi.org/10.1115/1.4029643
78. Lehn A, Mahner M, Schweizer B (2018) Characterization of static air foil thrust bearing performance: an elasto-gasdynamic analysis for aligned, distorted and misaligned operating conditions. Arch Appl Mech 88:705–728. https://doi.org/10.1007/s00419-017-1337-7
79. Basumatary KK, Kumar G, Kalita K, Kakoty SK (2020) Stability analysis of rigid rotors supported by gas foil bearings coupled with electromagnetic actuators. Proc Inst Mech Eng C J Mech Eng Sci 234:427–443. https://doi.org/10.1177/0954406219877903
80. Dutt JK, Nakra BC (1992) Stability of rotor systems with viscoelastic supports. J Sound Vib 153:89–96. https://doi.org/10.1016/0022-460X(92)90629-C
81. Kulkarni P, Pannu S, Nakra BC (1993) Unbalance response and stability of a rotating system with viscoelastically supported bearings. Mech Mach Theory 28:427–436. https://doi.org/10.1016/0094-114X(93)90081-6
82. Dutt JK, Nakra BC (1993) Vibration response reduction of a rotor shaft system using viscoelastic polymeric supports. J Vib Acoust 115:221–223. https://doi.org/10.1115/1.2930334
83. Dutt JK, Nakra BC (1995) Dynamics of rotor shaft system on flexible supports with gyroscopic effects. Mech Res Commun 22:541–545. https://doi.org/10.1016/0093-6413(95)00059-3
84. Montagnier O, Hochard Ch (2007) Dynamic instability of supercritical driveshafts mounted on dissipative supports—effects of viscous and hysteretic internal damping. J Sound Vib 305:378–400. https://doi.org/10.1016/j.jsv.2007.03.061
85. Shabaneh NH, Zu JW (2000) Dynamic analysis of rotor–shaft systems with viscoelastically supported bearings. Mech Mach Theory 35:1313–1330. https://doi.org/10.1016/S0094-114X(99)00078-6
86. Reddy MR, Srinivas J (2016) Vibration analysis of a support excited rotor system with hydrodynamic journal bearings. Procedia Eng 144:825–832. https://doi.org/10.1016/j.proeng.2016.05.093
87. Ribeiro EA, Alves DS, Cavalca KL, Bavastri CA (2021) Stability analysis and optimization of a hybrid rotating machinery support combining journal bearings with viscoelastic supports. Mech Mach Theory 156:104166. https://doi.org/10.1016/j.mechmachtheory.2020.104166
88. Ramesh J, Majumdar BC (1995) Stability of rough journal bearings using nonlinear transient method. J Tribol 117:691–695. https://doi.org/10.1115/1.2831538
89. Turaga R, Sekhar AS, Majumdar BC (2000) Non-linear transient stability analysis of a rigid rotor supported on hydrodynamic journal bearings with rough surfaces. Tribol Trans 43:447–452. https://doi.org/10.1080/10402000008982362
90. Lin J-R (2007) Application of the Hopf bifurcation theory to limit cycle prediction of short journal bearings with isotropic roughness effects. Proc Inst Mech Eng Part J J Eng Tribol 221:869–879. https://doi.org/10.1243/13506501JET310
91. Lin J-R (2014) The influences of longitudinal surface roughness on sub-critical and super-critical limit cycles of short journal bearings. Appl Math Model 38:392–402. https://doi.org/10.1016/j.apm.2013.06.024
92. Sinhasan R, Goyal KC (1995) Transient response of a two-lobe journal bearing lubricated with non-Newtonian lubricant. Tribol Int 28:233–239. https://doi.org/10.1016/0301-679X(95)00007-Q
93. Jagadeesha KM, Nagaraju T, Sharma SC, Jain SC (2012) 3D surface roughness effects on transient non-Newtonian response of dynamically loaded journal bearings. Tribol Trans 55:32–42. https://doi.org/10.1080/10402004.2011.626144
94. Kushare PB, Sharma SC (2014) Nonlinear transient stability study of two lobe symmetric hole entry worn hybrid journal bearing operating with non-Newtonian lubricant. Tribol Int 69:84–101. https://doi.org/10.1016/j.triboint.2013.08.014
95. Wang L, Snidle RW, Gu L (2000) Rolling contact silicon nitride bearing technology: a review of recent research. Wear 246:159–173. https://doi.org/10.1016/S0043-1648(00)00504-4
96. Tiwari M, Gupta K, Prakash O (2000) Dynamic response of an unbalanced rotor supported on ball bearings. J Sound Vib 238:757–779. https://doi.org/10.1006/jsvi.1999.3108
97. Gupta TC, Gupta K, Sehgal DK (2011) Instability and chaos of a flexible rotor ball bearing system: an investigation on the

influence of rotating imbalance and bearing clearance. J Eng Gas Turbines Power 133:082501. https://doi.org/10.1115/1.4002657
98. Harsha SP, Kankar PK (2004) Stability analysis of a rotor bearing system due to surface waviness and number of balls. Int J Mech Sci 46:1057–1081. https://doi.org/10.1016/j.ijmecsci.2004.07.007
99. Harsha SP (2005) Non-linear dynamic response of a balanced rotor supported on rolling element bearings. Mech Syst Signal Process 19:551–578. https://doi.org/10.1016/j.ymssp.2004.04.002
100. Chen G (2009) Study on nonlinear dynamic response of an unbalanced rotor supported on ball bearing. J Vib Acoust 131:061001. https://doi.org/10.1115/1.3142883
101. Ashtekar A, Sadeghi F (2011) Experimental and analytical investigation of high speed turbocharger ball bearings. J Eng Gas Turbines Power. https://doi.org/10.1115/1.4004004
102. Alfares MA, Elsharkawy AA (2003) Effects of axial preloading of angular contact ball bearings on the dynamics of a grinding machine spindle system. J Mater Process Technol 136:48–59. https://doi.org/10.1016/S0924-0136(02)00846-4
103. Changqing B, Qingyu X (2006) Dynamic model of ball bearings with internal clearance and waviness. J Sound Vib 294:23–48. https://doi.org/10.1016/j.jsv.2005.10.005
104. Bai C, Zhang H, Xu Q (2008) Effects of axial preload of ball bearing on the nonlinear dynamic characteristics of a rotor-bearing system. Nonlinear Dyn 53:173–190. https://doi.org/10.1007/s11071-007-9306-2
105. Gunduz A, Dreyer JT, Singh R (2012) Effect of bearing preloads on the modal characteristics of a shaft-bearing assembly: experiments on double row angular contact ball bearings. Mech Syst Signal Process 31:176–195. https://doi.org/10.1016/j.ymssp.2012.03.013
106. Conley B, Sadeghi F, Griffith RC, McCormack JW (2019) Experimental investigation of the dynamic loads in a ball bearing turbocharger. J Tribol 141:111101. https://doi.org/10.1115/1.4044296
107. Conley B, Sadeghi F (2021) Experimental and analytical investigation of turbocharger whirl and dynamics. Tribol Trans 64:239–252. https://doi.org/10.1080/10402004.2020.1827106
108. Conley B, Sadeghi F (2023) Impact of whirl and axial motion on ball bearing turbocharger dynamics. Tribol Trans 66:338–349. https://doi.org/10.1080/10402004.2022.2153774
109. San Andrés L, Yu F, Gjika K (2018) On the influence of lubricant supply conditions and bearing configuration to the performance of (semi) floating ring bearing systems for turbochargers. J Eng Gas Turbines Power 140:032503. https://doi.org/10.1115/1.4037920
110. Porzig D, Raetz H, Schwarze H, Seume JR (2014) Thermal analysis of small high-speed floating-ring journal bearings. In: 11th International conference on turbochargers and turbocharging. Elsevier, pp 421–436. https://doi.org/10.1533/978081000342.421
111. Liu Z, Wang R, Cao F, Shi P (2020) Dynamic behaviour analysis of turbocharger rotor-shaft system in thermal environment based on finite element method. Shock Vib 2020:1–18. https://doi.org/10.1155/2020/8888504
112. Trippett RJ, Li DF (1984) High-speed floating-ring bearing test and analysis. ASLE Trans 27:73–81. https://doi.org/10.1080/05698198408981547
113. Clarke DM, Fall C, Hayden GN, Wilkinson TS (1992) A steady-state model of a floating ring bearing, including thermal effects. J Tribol 114:141–149. https://doi.org/10.1115/1.2920852
114. Clarke DM, Fall C, Hayden GN, Wilkinson TS (1987) An analysis of the steady-state performance of the cylindrical-spherical floating ring bearing. J Tribol 109:704–708. https://doi.org/10.1115/1.3261541
115. San Andrés L, Kerth J (2004) Thermal effects on the performance of floating ring bearings for turbochargers. Proc Inst Mech Eng Part J J Eng Tribol 218:437–450. https://doi.org/10.1243/1350650042128067
116. San Andrés L, Barbarie V, Bhattacharya A, Gjika K (2012) On the effect of thermal energy transport to the performance of (semi) floating ring bearing systems for automotive turbochargers. J Eng Gas Turbines Power 134:102507. https://doi.org/10.1115/1.4007059
117. Li Y, Liang F, Zhou Y et al (2017) Numerical and experimental investigation on thermohydrodynamic performance of turbocharger rotor-bearing system. Appl Therm Eng 121:27–38. https://doi.org/10.1016/j.applthermaleng.2017.04.041
118. Liang F, Li Y, Zhou M et al (2017) Integrated three-dimensional thermohydrodynamic analysis of turbocharger rotor and semi-floating ring bearings. J Eng Gas Turbines Power 139:082501. https://doi.org/10.1115/1.4035735
119. San Andrés L, Jung W, Hong S-K (2021) A thermo-hydrodynamic model for thermal energy flow management in a (semi) floating ring bearing system for automotive turbochargers. J Eng Gas Turbines Power 143:011013. https://doi.org/10.1115/1.4048800
120. Lee D, Kim D (2010) Thermohydrodynamic analyses of bump air foil bearings with detailed thermal model of foil structures and rotor. J Tribol 132:021704. https://doi.org/10.1115/1.4001014
121. San Andrés L, Kim TH (2010) Thermohydrodynamic analysis of bump type gas foil bearings: a model anchored to test data. J Eng Gas Turbines Power 132:042504. https://doi.org/10.1115/1.3159386
122. San Andrés L, Ryu K, Kim TH (2011) Thermal management and rotordynamic performance of a hot rotor-gas foil bearings system—part I: measurements. J Eng Gas Turbines Power 133:062501. https://doi.org/10.1115/1.4001826
123. San Andrés L, Ryu K, Kim TH (2011) Thermal management and rotordynamic performance of a hot rotor-gas foil bearings system—part II: predictions versus test data. J Eng Gas Turbines Power 133:062502. https://doi.org/10.1115/1.4001827
124. Lee D, Kim D (2011) Three-dimensional thermohydrodynamic analyses of rayleigh step air foil thrust bearing with radially arranged bump foils. Tribol Trans 54:432–448. https://doi.org/10.1080/10402004.2011.556314
125. Aksoy S, Aksit MF (2015) A fully coupled 3D thermo-elasto-hydrodynamics model for a bump-type compliant foil journal bearing. Tribol Int 82:110–122. https://doi.org/10.1016/j.triboint.2014.10.001
126. Lehn A, Mahner M, Schweizer B (2018) A thermo-elasto-hydrodynamic model for air foil thrust bearings including self-induced convective cooling of the rotor disk and thermal runaway. Tribol Int 119:281–298. https://doi.org/10.1016/j.triboint.2017.08.015
127. Kumar J, Khamari DS, Behera SK, Sahoo RK (2022) Investigation of thermohydrodynamic behaviour of gas foil journal bearing accounting slip-flow phenomenon. J Braz Soc Mech Sci Eng 44:24. https://doi.org/10.1007/s40430-021-03330-9
128. Zhang J, Qiao X, Chen W et al (2022) Numerical investigation of thermo-aerodynamic characteristics of gas foil thrust bearing. Therm Sci Eng Prog 31:101296. https://doi.org/10.1016/j.tsep.2022.101296
129. Dellacorte C, Lukaszewicz V, Valco MJ et al (2000) Performance and durability of high temperature foil air bearings for oil-free turbomachinery. Tribol Trans 43:774–780. https://doi.org/10.1080/10402000008982407
130. Howard S, Dellacorte C, Valco MJ et al (2001) Dynamic stiffness and damping characteristics of a high-temperature air foil journal

bearing. Tribol Trans 44:657–663. https://doi.org/10.1080/10402000108982507
131. Howard SA, Dellacorte C, Valco MJ et al (2001) Steady-state stiffness of foil air journal bearings at elevated temperatures. Tribol Trans 44:489–493. https://doi.org/10.1080/10402000108982486
132. San Andrés L, Ryu K, Kim TH (2011) Identification of structural stiffness and energy dissipation parameters in a second generation foil bearing: effect of shaft temperature. J Eng Gas Turbines Power 133:032501. https://doi.org/10.1115/1.4002317
133. Radil K, Zeszotek M (2004) An experimental investigation into the temperature profile of a compliant foil air bearing. Tribol Trans 47:470–479. https://doi.org/10.1080/05698190490501995
134. Peng Z-C, Khonsari MM (2006) A thermohydrodynamic analysis of foil journal bearings. J Tribol 128:534–541. https://doi.org/10.1115/1.2197526
135. Jang JY, Khonsari MM (2003) A generalized thermoelastic instability analysis. Proc R Soc Lond A 459:309–329. https://doi.org/10.1098/rspa.2002.1030
136. Dykas B, Howard SA (2004) Journal design considerations for turbomachine shafts supported on foil air bearings. Tribol Trans 47:508–516. https://doi.org/10.1080/05698190490493391
137. Zywica G, Baginski P, Kicinski J (2017) Selected operational Problems of high-speed rotors supported by gas foil bearings. Tech Mech 37(2–5):339–346. https://doi.org/10.24352/UB.OVGU-2017-109
138. Lee D, Kim D, Sadashiva RP (2011) Transient thermal behavior of preloaded three-pad foil bearings: modeling and experiments. J Tribol 133:021703. https://doi.org/10.1115/1.4003561
139. Samanta P, Khonsari MM (2018) On the thermoelastic instability of foil bearings. Tribol Int 121:10–20. https://doi.org/10.1016/j.triboint.2018.01.014
140. Heshmat H, Walton JF, Tomaszewski MJ (2005) Demonstration of a Turbojet engine using an air foil bearing. In: Volume 1: turbo expo 2005. ASMEDC, Reno, Nevada, USA, pp 919–926
141. Mutra RR, Srinivas J (2022) An optimization-based identification study of cylindrical floating ring journal bearing system in automotive turbochargers. Meccanica 57:1193–1211. https://doi.org/10.1007/s11012-022-01507-7